water

MDPI

Article

Evaluating Performances of LSTM, SVM, GPR, and RF for Drought Prediction in Norway: A Wavelet Decomposition Approach on Regional Forecasting

Sertac Oruc [1,2,*], Mehmet Ali Hinis [3] and Turker Tugrul [4]

[1] The Center for Sámi Studies, UiT Norges Arktiske Universitet, N-9037 Tromsø, Norway
[2] Civil Engineering Department, Faculty of Engineering and Natural Sciences, 15 Temmuz Şehitleri Campus, Ankara Yıldırım Beyazıt University, Ankara 06010, Türkiye
[3] Civil Engineering Department, Faculty of Engineering, Central Campus, Aksaray University, Aksaray 68100, Türkiye; mhinis@aksaray.edu.tr
[4] Research Development Institution Office, Central Campus, Gazi University, Ankara 06560, Türkiye; turkertugrul@gazi.edu.tr
* Correspondence: seoru2529@uit.no or sertacoruc@aybu.edu.tr

Abstract: A serious natural disaster that poses a threat to people and their living spaces is drought, which is difficult to notice at first and can quickly spread to wide areas through subtle progression. Numerous methods are being explored to identify, prevent, and mitigate drought, and distinct metrics have been developed. In order to contribute to the research on measures to be taken against drought, the Standard Precipitation Evaporation Index (SPEI), one of the drought indices that has been developed and accepted in recent years and includes a more comprehensive drought definition, was chosen in this study. Machine learning and deep learning algorithms, including support vector machine (SVM), random forest (RF), long short-term memory (LSTM), and Gaussian process regression (GPR), were used to model the droughts in six regions of Norway: Bodø, Karasjok, Oslo, Tromsø, Trondheim, and Vadsø. Four distinct model architectures were employed for this goal, and as a novel approach, the models' output was enhanced by using discrete wavelet decomposition/transformation (WT). The model outputs were evaluated using the correlation coefficient (r), Nash–Sutcliffe efficiency (NSE), and root mean square error (RMSE) as performance evaluation criteria. When the findings were analyzed, the GPR model (W-GPR), which was acquired after WT, typically produced the best results. Furthermore, it was discovered that, out of all the recognized models, M04 had the most effective model structure. Consequently, the most successful outcomes were obtained with W-SVM-M04 for Bodø and W-GPR-M04 for Karasjok, Oslo, Tromsø, Trondheim, and Vadsø. Furthermore, W-GPR-M04 in the Oslo region had the best results across all regions (r: 0.9983, NSE: 0.9966 and RMSE:0.0539).

Keywords: global change; extreme weather; machine learning; deep learning; risk assessment; SPEI

Citation: Oruc, S.; Hinis, M.A.; Tugrul, T. Evaluating Performances of LSTM, SVM, GPR, and RF for Drought Prediction in Norway: A Wavelet Decomposition Approach on Regional Forecasting. *Water* **2024**, *16*, 3465. https://doi.org/10.3390/w16233465

Academic Editor: Maria Mimikou

Received: 4 November 2024
Revised: 25 November 2024
Accepted: 27 November 2024
Published: 2 December 2024

1. Introduction

Climate change mainly caused by human activities possesses a significant threat to the environment and economic development. The Intergovernmental Panel on Climate Change (IPCC) 6th Assessment Report [1] indicates the acceleration of climate change with the consequences such as rising global temperatures and an increase in extreme rainfall events. This phenomenon could be explained by the increased moisture capacity of the warmer atmosphere. While a hotter and wetter future is projected globally, regional differences must also be considered, as some regions may experience these changes more intensely than others.

Droughts, characterized by extended periods of below-average precipitation, lead to profound impacts across various sectors including agriculture, water supply, and ecosystems, causing both direct and indirect effects such as lower crop yield, water scarcity, and

extreme events such as wildfires [2,3]. In our water-dependent society, the economic and environmental impacts are among the highest of natural hazards, with the potential for conflicts over water resources, increasing with the severity of droughts [4–7]. Particularly in Northern Europe, including Norway, the region is experiencing particularly notable climatic shifts, with projections indicating more severe droughts and hotter summers due to climate change [8–10].

Studies using hydrological modeling and climate projections suggest that droughts will become more frequent, severe, and persistent, particularly affecting the water, energy, food, and ecosystem sectors within these northern territories [6,11]. Additionally, shifts in precipitation patterns are expected, with notable decreases in winter and increases in summer, complicating water management and elevating the likelihood of drought-related challenges [12]. To sustain vital ecosystem services and ensure social prosperity within rapidly changing regions, a comprehensive understanding of and ability to predict these drought events is crucial [13]. This underscores the urgent need for enhanced drought prediction and management strategies to address water security and to mitigate the adverse impacts on society and the environment, particularly in the vulnerable northern regions of Europe.

Machine learning (ML) and deep learning (DL) models are widely recognized as advanced and powerful tools to utilize for making more accurate and region-specific predictions using observed climate data and exploring the predictability of climate systems. These techniques are utilized as predictive tools across various fields globally, supported by the increased availability of big data (Figure 1). The vast availability of big data in drought prediction greatly benefited researchers employing ML, contributing toward a sustainable ecosystem [14–16]. ML techniques such as the adaptive neuro-fuzzy inference system (ANFIS), artificial neural networks (ANN), random forest (RF), and support vector machines (SVM) gained widespread use in prediction models [17]. Machine learning methods excel at handling large datasets and complex analyses in climate science, effectively modeling intricate relationships in high-dimensional data, including missing values. These capabilities make them particularly well-suited for tackling complex, data-rich environments [18–20]. As a result, ML models have been successfully employed in environmental and natural hazard research, including tasks such as identifying areas prone to land subsidence, landslides, and extreme weather events, as well as flood and drought prediction [17,20].

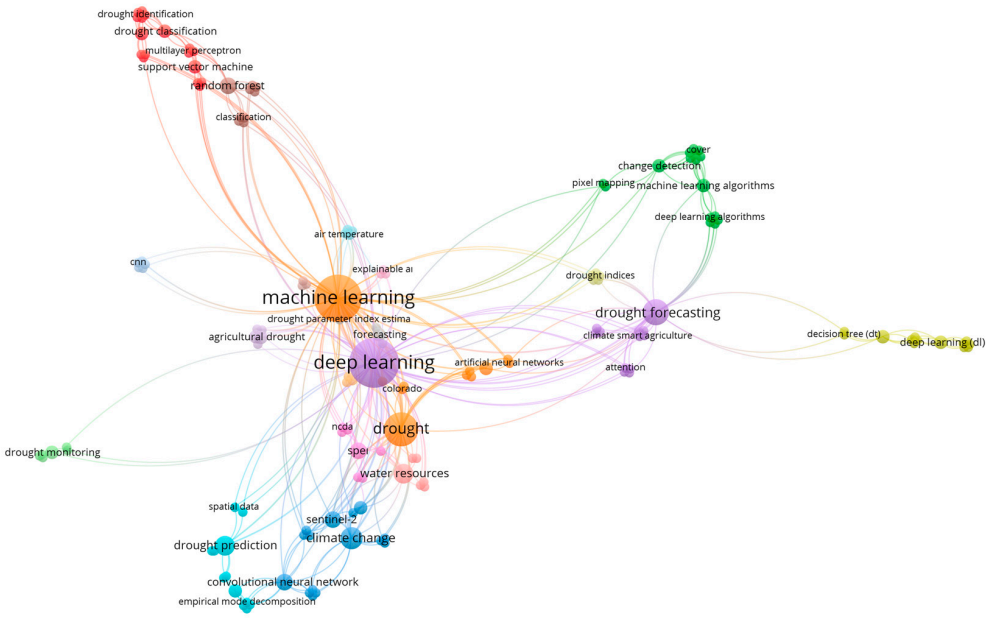

Figure 1. Wide use of machine and deep learning on climate system.

Recent advancements in ML have also been employed in drought prediction. For instance, Pande et al. [21] tested an improved SVM model and found varying levels of success with different kernel functions based on the time steps for predicting the standardized precipitation index (SPI) in the upper Godavari River basin. Emphasizing droughts as severe climatic events, Achite et al. [22] demonstrated that the extreme learning machines, including the wavelet decomposition (W-ELM) model, are reliable tools for predicting hydrological drought in the Wadi Mina Basin, Algeria. Moreover, Achite et al. [23] highlighted the need for extensive drought prediction studies in Mediterranean regions. They implemented a comprehensive suite of ML models and found wavelet-enhanced GPR models show significant potential in estimating drought indices effectively, establishing a foundation for future predictive endeavors in drought-prone areas. Pande et al. [24] initially calculated SPI3 and SPI6 to detect droughts in the region, utilizing monthly rainfall data from the River Godavari spanning from 1989 to 2019. Subsequently, six distinct models were developed to forecast drought in the study area and were examined using five different methods. The methods include SVM, bagged trees, boosted trees, robust linear regression, and Matern GPR. Ultimately, they concluded that the Matern GPR provides more precise results compared to other models in their findings. Latifoğlu et al. [25] are also one of the researchers who carried out drought studies utilizing the SPI and the standard precipitation evapotranspiration index (SPEI). Analyses were conducted employing ANN, SVM, and GPR methods, utilizing meteorological data from two distinct stations in the Euphrates basin spanning the years 1965 to 2022 and according to their results GPR demonstrated the most effective outcomes. Talebi et al. [26] carried out a study focused on predicting future droughts using MLP and RF techniques in Iran. Subsequently, these algorithms were integrated with the genetic algorithm (GA). In the analysis, they revealed that RF stands out as the superior algorithm compared to MLP.

Furthermore, among the deep learning models, the utilization of a dynamic recurrent neural network (RNN) and the long short-term memory model (LSTM) have been combined and applied in various locations with excellent results [27]. RNNs are designed to handle sequential data, making them particularly effective for time series analysis, which encompasses variables such as drought indices. RNN possess a hidden state that retains information from past sequences, enabling them to identify and learn from long-term patterns in the data. An LSTM network builds on this by incorporating the memory capability of an RNN. The main innovation of LSTM is its memory cell (ct), which stores state information. This cell is controlled by numerous self-parameterized control gates for access, modification, and clearance. When the input gate is active, the information from each new input is stored in the cell [28–30]. For problems that require the sequential order of inputs, the current state-of-the-art network design is the so-called LSTM, first introduced by Hochreiter and Schmidhuber [31]. The LSTM model addresses the issue faced by traditional RNNs in learning long-term dependencies, such as the storage effects observed in hydrological catchments. These effects are crucial in hydrological processes, particularly in snow-driven catchments [32].

As highlighted by Villegas-Ch and Garcia-Ortiz [33], LSTM has a proven ability to handle temporal sequences and store information over time, which is critical for understanding and predicting long-term climatic phenomena such as droughts. Wu et al. [34] used LSTM to build statistical models by means of meteorological variables as predictors and the SPI3. The results indicate that the LSTM models that accurately simulated SPI3 in the training, validation, and test sets utilizing ERA5 reanalysis data are highly accurate. Wang et al. [35] used the LSTM algorithm to predict and evaluate drought conditions using multiple source features, concluding that LSTM in conjunction with multi-source variables considerably improves the accuracy and reliability of drought prediction. Dikshit et al. [36] applied this deep learning approach, specifically LSTM, with a global climatological dataset to understand the predicting skills in terms of SPEI values and analyzed the variation in terms of drought categories and spatial variation. They concluded that this technique was more effective for forecasting than typical machine learning approaches. Kratzert et al. [32]

investigated the feasibility of using LSTM to simulate runoff from meteorological observations and demonstrated comparable performance to their baseline hydrological model (SAC-SMA + Snow-17). Phetanan et al. [37] also combined the SWAT and LSTM models to simulate water flow rates in a tidal river, highlighting the Soil and Water Assessment Tool (SWAT) with LSTM (SWAT-LSTM) model's potential for accurate and efficient simulation of water flow rates in tidal river systems. The promising performance of those LSTM models lends credence to their utility in researching the predictability of climate systems and developing predictions using observed climate data. Taylan [38] explored the potential of LSTM by using SPI for forecasting drought in Türkiye and underlined the efficacy of LSTM, a deep learning technique, in drought research and verified the excellent outcomes.

Additionally, wavelet transform/decomposition (WT) has proven to be effective in enhancing the performance of these models. Belayneh et al. [39], for instance, enhanced SVM and ANN with WT preprocessing and observed that the artificial neural networks paired with WT (W-ANN) outperformed the support vector machines coupled with WT (W-SVM) in predicting SPI values in the Awash River Basin, Ethiopia. Deo and Şahin [40] predicted droughts using ANN for SPEI in Eastern Australia, with data spanning from 1915 to 2012, where the multi-layer perceptron (MLP) model demonstrated superior performance. Particle Swarm Optimization (PSO) and the Response Surface Method (RSM) are also commonly incorporated into SVM in addition to ANN. Piri et al. [41] recently conducted a comparative analysis of four machine learning models to investigate the predictability capabilities in meteorological drought indices and revealed that SVR-RSM demonstrated superior accuracy and trend detection compared to other models, while SVR-PSO outperformed ANN and standard SVR. Tuğrul and Hinis [16] conducted a study on drought forecasting by using various ML algorithms, SVM, ANN, decision tree (DT), and random forest (RF), in the Apa Dam. WT in their study was also applied to improve models' performances with RF and W-SVM showing superior performance. Highlighting agriculture, meteorological, and hydrological droughts as natural hazards, Elbeltagi et al. [42] investigated potential future droughts with the help of RF, random tree (RT), and Gaussian process regression (GPR) models for the study area of India. Their results suggest that the RF was the most effective model for forecasting droughts compared to the others.

This study compares five different methods considering their drought prediction capabilities, combining machine learning and signal processing techniques, to assess their effectiveness and suitability for diverse regional contexts in six locations (Oslo, Tromsø, Vadsø, Trondheim, Bodø, and Karasjok) of Norway. The four methods under investigation include LSTM: a recurrent neural network adept at capturing long-term dependencies in sequential data, making it well-suited for forecasting drought index values and capturing seasonal effects [28,32]. SVM: a robust supervised learning model capable of handling complex relationships between climate variables, making it suitable for both drought classification and severity prediction, even with limited data. GPR: it is a model based on probability theorems, where some of its variables exhibit a multivariate Gaussian distribution [23,43]. RF: it is a supervised machine learning method used in both classification and regression [44,45]. Additionally, these four methods will be coupled with wavelet decomposition (WT): a versatile signal processing technique capable of capturing both high-frequency and low-frequency patterns in climate data, making it suitable for preprocessing data to enhance the performance of various drought forecasting models, including SVM and LSTM [46].

Upon reviewing the literature, it becomes evident that the methods employed align closely with those utilized in this study. However, a crucial aspect to consider is the integration of the utilized methods in this study with the chosen transfer method, wavelet, and the subsequent comparison of the results. This study employed four distinct algorithms, utilizing WT to enhance the model outcomes, showcasing the article's originality.

The aim of this study is to comprehensively evaluate and compare the effectiveness of four advanced machine learning and signal processing techniques, LSTM, SVM, GPR, and RF, each integrated with WT, for predicting droughts in various regions of Norway.

The study aims to assess the strengths and weaknesses of each method and determine their suitability for different drought forecasting contexts in each region, with the ultimate goal of enhancing the accuracy and reliability of drought predictions, thereby providing valuable insights for water resource management, agricultural planning, risk assessment, and ecological conservation efforts in the study area.

2. Methodology

This work presents an analysis of SPEI data collected from six distinct locations of Norway. The analysis used a range of machine and deep learning methods implemented within four different model architectures. In this study, the algorithms implemented include SVM, RF, GPR, and LSTM. Upon completing the analyses, WT was paired to enhance the performance of the results. The methodological framework in this study is summarized graphically in Graphical abstract.

2.1. Study Region and Data

The study encompasses six diverse regions across Norway, each characterized by distinct geographical and climatic conditions that influence their drought forecasting needs (Figure 2). These regions include Oslo, Tromsø, Vadsø, Trondheim, Bodø, and Karasjok, spanning from the southern lowlands to the northernmost points of the country. Norway's climate is predominantly maritime, strongly influenced by its latitude and extensive coastline, with the Gulf Stream bringing milder air to its shores. Oslo, the capital, experiences a humid continental climate, with relatively warm summers and cold winters, making it critical to evaluate drought impacts on both urban and surrounding agricultural areas. Moving north to Tromsø and Vadsø, the climate shifts to subarctic, where winters are longer and harsher, and summers are milder and shorter, shaping the seasonal dynamics of drought risk. Trondheim and Bodø, with their proximity to the sea, experience a more temperate oceanic climate, which can lead to varied precipitation patterns and influence drought frequency and severity. Karasjok, in the far north, lies well within the Arctic Circle and constitutes an entirely different climate regime, characterized by very cold winters and brief, mild summers, posing specific challenges for drought forecasting. By examining these varied regions, the study aims to encapsulate the wide array of climate conditions present in Norway (Table 1), ensuring that the drought prediction methods evaluated can be adapted to the diverse environmental circumstances found throughout the country.

Table 1. Data statistics.

Data Location Point	Inıtial	End	Type of Data	Min	Max	Latitude	Longitude
Bodø	12-1901	12-2022	SPEI12	−2.8	2.4	67.280324	14.404921
Karasjok	12-1901	12-2022	SPEI12	−2.3	2.5	69.471924	25.510800
Oslo	12-1901	12-2022	SPEI12	−3.2	2.7	59.913779	10.752332
Tromsø	12-1901	12-2022	SPEI12	−2.6	2.6	69.676441	18.975012
Trondheim	12-1901	12-2022	SPEI12	−2.6	2.4	63.430426	10.394946
Vadsø	12-1901	12-2022	SPEI12	−2.2	2.3	70.077335	29.748846

Data could have been collected using remote sensing methods, models, and analyses, which are often favored in the literature [47]. However, SPEI data were collected directly from The Global SPEI database, https://spei.csic.es/spei_database (accessed on 1 September 2024), SPEI-base, which offers long-time, robust information about drought conditions at the global scale, with a 0.5 degrees' spatial resolution and a monthly time resolution [48]. It has a multi-scale character, providing SPEI timescales ranging from 1 to 48 months. It is based on monthly precipitation and potential evapotranspiration data from the Climatic Research Unit of the University of East Anglia, starting in January 1901.

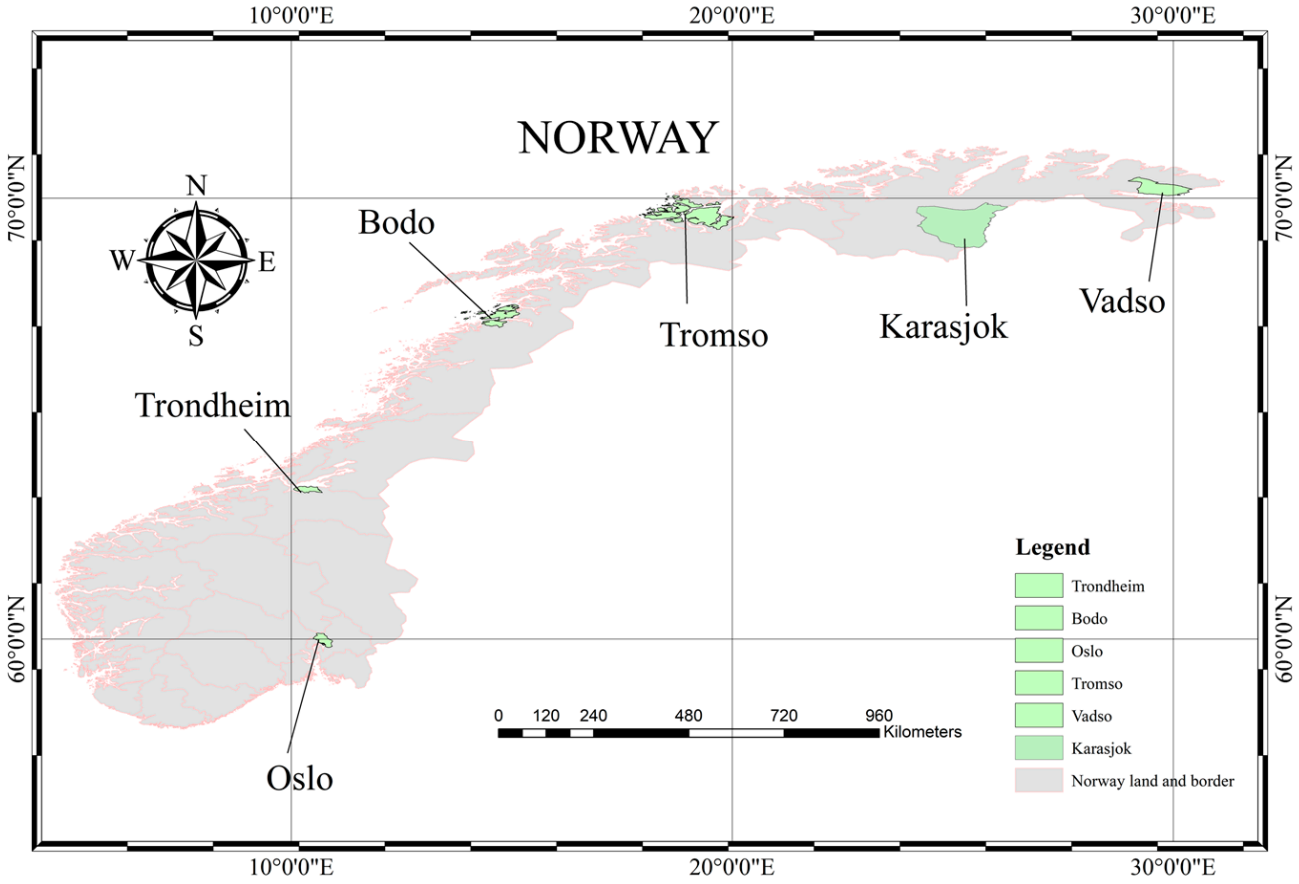

Figure 2. Study area.

2.2. Standard Precipitation Evapotranspiration Index (SPEI)

It is important to choose appropriate drought indicators based on the region's climate and environmental conditions [49]. For instance, SPI is suitable for regions where drought is primarily caused by a lack of precipitation, while SPEI performs better in areas where temperature variations also play a significant role [49–51]. The inclusion of temperature variability makes SPEI particularly relevant in the context of climate change.

SPEI, a relatively new meteorological drought index, incorporates SPI's strengths while also taking into account the temperature variability [51]. The SPEI's calculation process, as described by Vicente-Serrano et al. (2010), involves first determining the potential evapotranspiration (*PET*) for each month, followed by calculating the monthly water balance deficit (D_i) by subtracting PET from the precipitation value (P_i) [51,52].

$$D_i = P_i - PET_i \quad (1)$$

This process ensures that SPEI can account for both precipitation and temperature influences [53], making it more suitable for drought monitoring under changing climate conditions [54]. The inclusion of additional sources such as Hao and Singh [55], Haro-Monteagudo et al. [56], and Wahla et al. [52] enhances the credibility and depth of the analysis.

SPEI calculations follow the same basic steps as in the SPI, transforming the log-logistic distribution to a standard normal distribution. For details of the method, please refer to Vicente-Serrano et al. [57].

PET values are the most important parameter that distinguishes the SPI method from the SPEI method. The calculation of the PET value, which is required in addition to the precipitation for the calculation of D_i, can directly affect the results [58]. The SPEI-base site, where the SPEI values are taken, uses the FAO-56 Penman-Monteith (PM) method,

which gives the most accurate results for PET calculations. FAO56-PM is presented in Allen et al. [59] as follows:

$$ET_{pm} = (0.408\Delta(R_n - G) + \gamma(900/(T + 273))U_2(e_s - e_a))/(\Delta + \gamma(1 + 0.34U_2)) \quad (2)$$

where ET_{pm} is reference evapotranspiration (mm day^{-1}), Δ is the slope of the saturation vapor pressure function (kPa °C^{-1}), γ is psychometric constant (kPa °C^{-1}), R_n is net radiation (MJ m^{-2} day^{-1}), G is soil heat flux density (MJ m^{-2} day^{-1}), T is mean air temperature (°C), U_2 is average 24 h wind speed at 2 m height (m s^{-1}), e_s is saturation vapor pressure (kPa), and e_a is actual vapor pressure (kPa) [60].

In this study, all data were normalized before training the relevant machine learning on all models. Then the analysis results were evaluated according to the results that obtained from the test data. After all the processes were completed, the data were restored to their previous state by applying de-normalization.

$$D = \sum_{i=1}^{k} \frac{N_i - \overline{N}}{N_{max} - N_{min}} \quad (3)$$

where D is the normalized value, $\overline{N}$ represents mean in dataset, N_{max} is the maximum value, and N_{min} is the minimum value.

2.3. Long Short-Term Memory Network (LSTM)

In recent years, deep learning has seen significant advances within the realm of artificial intelligence, notably in areas such as image classification and time series prediction. The long short-term memory (LSTM) model, an evolution/improvement over the standard recurrent neural network (RNN), effectively addresses the issue of vanishing gradients common in traditional RNNs. LSTM achieves this by incorporating mechanisms that allow it to process information across extended time intervals, as proposed by Hochreiter and Schmidhuber [31]. The strength of the LSTM lies in its capability to maintain long-term data sequences through enhanced memory components, such as memory cells and various gates, making it more efficient for handling prolonged sequences compared to standard RNNs [61].

The architecture of an LSTM network includes a sequence input (SI) layer, essential for feeding time series data into the network. This layer connects to the LSTM layer, composed of units that feature an input gate, a forget gate, a cell with a self-recurrent connection, and an output gate. These components collectively manage the information by adding or removing it as necessary, a concept pioneered by Hochreiter and Schmidhuber [31]. To optimize the LSTM parameters and minimize the loss function, various algorithms such as stochastic gradient descent (SGD), root mean square propagation (RMSProp), and adaptive moments (Adam) can be employed. Similar to RNNs, LSTMs compute a mapping from an input sequence x to an output sequence y by calculating the network unit activations using the following equations iteratively from $t = 1$ to $t = \tau$ with initial values $C_0 = 0$ and $h_0 = 0$:

$$i_t = \sigma(W_i\, x_t + U_i\, h_{t-1} + b_i) \quad (4)$$

$$f_t = \sigma\left(W_f\, x_t + U_f\, h_{t-1} + b_f\right) \quad (5)$$

$$o_t = \sigma(W_o\, x_t + U_o\, h_{t-1} + b_o) \quad (6)$$

$$C_t = tanh(W_c\, x_t + U_c\, h_{t-1} + b_c) \quad (7)$$

$$C_t = f_t \otimes\, C_{t-1} + i_t \otimes\, C_t \quad (8)$$

$$h_t = o_t \otimes\, tanh(C_t) \quad (9)$$

where W_i, W_f, and W_o denote the matrix of weights from the input, forget, and output gates to the input, respectively. In the architecture of LSTM networks, U_i, U_f, and U_o represent

the weight matrices connecting the input, forget, and output gates to the hidden layer, respectively. Similarly, b_i, b_f, and b_o are the bias vectors for the input, forget, and output gates. The σ denotes a logistic sigmoid function used as a non-linear activation function applied element-wise. The vectors i_t, f_t, o_t, and C_t correspond to the input, forget, output gates, and the cell state at any given time stamp t, all of which are dimensionally equivalent to the cell output vector, h_t. The operation $\otimes$ symbolizes the element-wise multiplication between two vectors. For a more comprehensive understanding of LSTM networks and their mechanisms, references such as Kratzert et al. [32], Zhang et al. [28], Dikshit et al. [36], and Wang et al. [35] provide in-depth discussions and analyses.

2.4. Support Vector Machine (SVM)

The support vector machine (SVM) was developed in 1992 by Boser et al. [62], and is extensively employed for classification and regression tasks, markedly enhancing predicted accuracy in hydrology and other domains based on the statistical learning theory. The support vector machine (SVM) is a supervised learning technology which distinguishes itself by providing a singular, optimal solution for a specific dataset, unlike other algorithms that may yield several answers. This characteristic renders SVM very proficient in mitigating overfitting by employing a kernel function to establish decision boundaries in nonlinear scenarios [63].

The support vector machine (SVM) is a classifier that belongs to the kernel approaches in machine learning. This learning system is employed to classify and predict the data fitness function, aiming to minimize mistakes in data categorization or the fitness function itself. In linear data classification, the objective is to identify a line that possesses a more robust margin [64].

Owing to its adaptability and efficacy, SVM is extensively utilized for both regression and classification, positioning it as a premier method in machine learning, with a multitude of successful applications. Its adaptability has been thoroughly examined, with numerous adjustments producing favorable results [23,65,66].

In the context of regression issues, SVM is designated as support vector regression (SVR) [67,68]. The principal objective of SVM is to reduce statistical learning mistakes, hence enhancing the model's predictability and robustness [39]. Gunn [69], Vapnik [70], and Panahi et al. [71] provide a brief description of the theory behind support vector regression.

The efficacy of SVM models is contingent upon the selection of kernel function, including linear, polynomial, radial basis function (RBF), sigmoid, or Gaussian. This study selected the Gaussian kernel because of its substantial influence on model performance. Three critical parameters directly affect the model's performance with the Gaussian kernel: the scale parameter (γ), the regularization constant (C), and epsilon (ε), as articulated by Belayneh et al. [72]. The parameters were automatically tuned in MATLAB to improve the model's efficacy.

The mathematical formulation of SVM is presented in Equation (10), defining the relationship between input and output variables:

$$f(x) = (w, \phi(x)) + b \tag{10}$$

where $f(x)$ denotes a high dimensional feature space, w represents a weight of the output variable, and b refers to the bias term.

2.5. Gaussian Process Regression (GPR)

Gaussian processes (GPs) offer a powerful and flexible approach to regression and classification problems, moving beyond the limitations of simple parametric forms. Their strength lies in their non-parametric nature, allowing them to model complex relationships within data by defining a distribution over functions rather than just parameters [73].

A key feature of GPs is the wide array of covariance functions available. These functions determine the degrees and characteristics of the modeled functions, enabling

researchers to tailor the GP to the specific structure of their data [73,74]. This flexibility makes GPs particularly well-suited for addressing diverse engineering and modeling challenges [75].

Gaussian process regression (GPR) leverages this concept by assuming that past observations contain valuable information about future ones and, unlike the Gaussian distribution, the Gaussian process is over functions [76]. This data-driven, non-parametric approach allows GPR to model complex relationships without the need for explicit model validation to generalize them [76,77].

Several advantages make GPR appealing for various applications, including easy implementation, adaptable hyperparameter tuning, and the ability to provide probabilistic predictions, quantifying uncertainty in a statistically sound manner [42,78]. This led to a surge in interest in GPR from both industry and academia. Notably, specialized kernels such as the PUK kernel, designed for large datasets, further expanded the applicability of GPR in fields such as hydrology and climate research [42,78].

2.6. Random Forest

Random forest (RF), developed by Breiman [79], is a machine learning technique used for both the classification and the regression tasks [45]. By utilizing a single data set, multiple models are trained, which also increases the prediction accuracy. This consists of three key steps, such as data subdivision, obtaining decision trees for these subdivisions, and development of the final prediction by averaging the predictions obtained from trees [45,80]. Random forest has several key advantages, such as high accuracy-low errors and computational speed as Choi et al. [81] indicated. Moreover, ease of hyper-parameter tuning during runtime is also an advantage for RF compared to ANN and SVR [45,82]. For more detail, readers can refer to Breiman [79], Biau and Scornet [83], Yu et al. [84], and Tyralis et al. [85].

2.7. Discrete Wavelet Transformation

Wavelet transform is typically presented in two versions in the literature: continuous wavelet transform (CWT) and discrete wavelet transform (DWT). Owing to the computational intricacies associated with the implementation of continuous wavelet transform (CWT), discrete wavelet transform (DWT) is frequently favored [86,87]. The discrete wavelet transform (DWT) offers an alternative to Fourier transform, decomposing time series data into sub-signals across different frequency components by employing signal processing, so that the extraction of specific features is enabled [88,89]. It offers a time-frequency analysis of a signal by employing a mathematical function to deconstruct it in the time domain.

The discrete wavelet transform employs a wavelet function, ψ_t, referred to as the "mother wavelet", which differentiates among various frequencies. It functions at several scales (s_0) and is temporally localized (τ_0). The calculation of mother wavelet is presented in Equation (11):

$$\psi_{m,n}(t) = \frac{1}{s_0^m}\psi\left\{\frac{t - n\tau_0 s_0^m}{s_0^m}\right\} \tag{11}$$

where m and n indicate controlling parameters of scale and time. The most common selections for the parameters S_0 and τ_0 are 2 and 1, respectively. Based on Mallat's theory [90], the discrete wavelet transform (DWT) can decompose a signal into its inverse DWT, resulting in a sequence of approximation and detail signals that are linearly independent. Here, S_0 refers to the step of precision expansion, while τ_0 denotes the location parameter for the DWT applied to a discrete time series x_i, where each x_i, occurs at a discrete time i. The inverse DWT, as described by Mallat [90], is expressed in Equation (12), which outlines the reconstruction process from these independent signals.

$$x(t) = T + \sum_{m=1}^{M}\sum_{t=0}^{2^{M-m-1}} W_{m,n}2^{-\frac{m}{2}}\psi(2^{-m}t - n) \tag{12}$$

where $W_{m,n}2^{-\frac{m}{2}}\sum_{t=0}^{N-1}\psi(2^{-m}t-n)x(t)$ is the wavelet coefficient for the discrete wavelet at scale $s=2^m$ and $\tau=2^m$. Five level detailed studies were chosen and employed in WT in this study since we obtained improved model results. The calculation of the level (L) is based on the Equation (13):

$$L = int(N) \tag{13}$$

where L is the level of the decomposition and N is the number of runs.

2.8. Model Performance Assessment

Model performance was evaluated using three well-known statistical metrics: the correlation coefficient (R), root mean square error (RMSE), and the Nash–Sutcliffe efficiency (NSE). These metrics are defined in Equations (14)–(16), respectively.

In Equations (14)–(17), SPI_{pi} = the predicted value, SPI_{oi} = the observed value, N = the number of data, $\overline{SPI_o}$ = average observed value, and $\overline{SPI_p}$ = average predicted value.

Correlation coefficient (R) can be calculated as in Equation (14) [91]:

$$R = \frac{\sum_{i=1}^{N}\left(SPI_{pi}-\overline{SPI_p}\right)\left(SPI_{oi}-\overline{SPI_o}\right)}{\sqrt{\sum_{i=1}^{N}\left(SPI_{pi}-\overline{SPI_p}\right)^2}*\sqrt{\sum_{i=1}^{N}\left(SPI_{oi}-\overline{SPI_o}\right)^2}}. \tag{14}$$

RMSE is calculated in Equation (15) [92]:

$$RMSE = \sqrt{\frac{1}{N}\sum_{i=0}^{N}\left(SPI_{oi}-SPI_{pi}\right)^2}. \tag{15}$$

NSE is calculated in Equation (16) [93]:

$$NSE = 1-\left[\frac{\sum_{i=1}^{N}\left(SPI_{oi}-SPI_{pi}\right)^2}{\sum_{i=1}^{N}\left(SPI_{oi}-\overline{SPI_o}\right)^2}\right]. \tag{16}$$

In addition to above metrics, a more robust comparative performance analyses were also demonstrated by using an RMSE-standard deviation ratio (RSR), as defined in Equation (17) [94].

$$RSR = \frac{\sqrt{\sum_{i=1}^{N}\left(SPI_{oi}-SPI_{pi}\right)^2}}{\sqrt{\sum_{i=1}^{N}\left(SPI_{oi}-\overline{SPI_o}\right)^2}} \tag{17}$$

2.9. Model Structure

In this study, the cross-correlation method was used to select the most appropriate model inputs, as emphasized in the literature [16,63]. In the literature, methods such as auto-correlation and cross-correlation, are preferred to select model input data. Cross-correlation engages with prior data more effectively than autocorrelation, highlighting the data that aligns most closely with the study needs. In other words, autocorrelation calculations are based on historical data closest to the output data, whereas cross-correlation involves interactions with all data in the dataset. As given in Figure 3, the most effective parameter on the output data are the data of time t-1, t-12, respectively. Based on the results obtained from cross-correlation (Figure 3), Table 2 presents the optimal input configuration for each of the four models considering the diverse features of the study area.

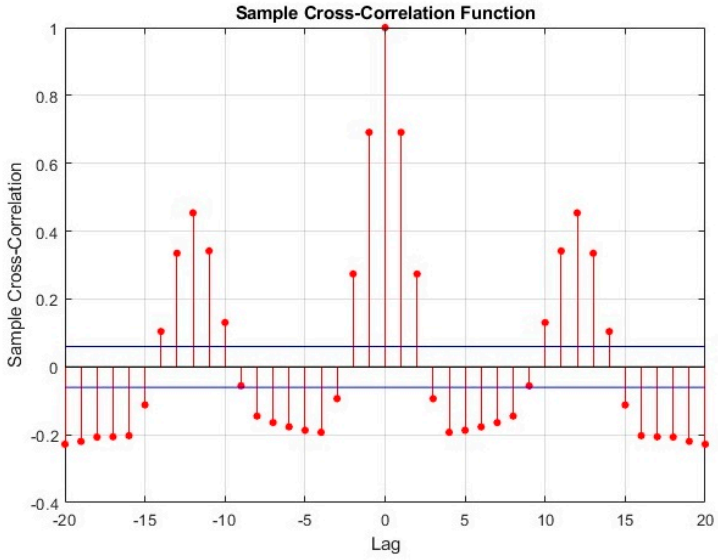

Figure 3. The results of cross-correlation for the most appropriate model inputs.

Table 2. Structure of models derived by cross-correlations based on SPEI12 values.

Model	Inputs							Output
M01	t-13	t-12	t-11	t-1				t
M02	t-2	t-13	t-12	t-11	t-1			t
M03	t-3	t-2	t-13	t-12	t-11	t-1		t
M04	t-4	t-3	t-2	t-13	t-12	t-11	t-1	t

3. Results and Discussion

This study employed the SPEI12 index to forecast future droughts as it effectively captures meteorological drought conditions [95]. Numerous researchers also consistently utilized SPEI12 for drought monitoring and prediction [16,63,96–99]. Four different models, for which were determined by cross-correlation of the input data, were analyzed with a series of machine learning methods and deep learning methods, SVM, RF, LSTM, and GPR, for the six different regions. Then, the models' performance was improved by means of WT. Consequently, the results of the analyses performed with the different models and algorithms are shown based on stations in Table 3. Table 3 serves the analysis results of all models using several machine learning techniques, including SVM and RF, as well as deep learning algorithms such as LSTM and GPR. The models that achieved the best results within their respective groups are indicated in bold. Additionally, all reviews in Table 3 were assessed individually for each station.

Table 3. Results of the testing data for all models and algorithms (Bolds indicate best performers).

Test Data	Bodø				Karasjok				Oslo			
Model		**r**	**NSE**	**RMSE**		**r**	**NSE**	**RMSE**		**r**	**NSE**	**RMSE**
M01	SVM	0.9408	0.8801	0.2882	SVM	0.9433	0.8850	0.2820	SVM	0.9475	0.8966	0.2952
	W-SVM	0.9782	0.9568	0.1731	W-SVM	0.9797	0.9593	0.1677	W-SVM	0.9788	0.9580	0.1883
	RF	0.9118	0.8103	0.3625	RF	0.9191	0.8232	0.3497	RF	0.9201	0.8343	0.3738
	W-RF	0.8744	0.7283	0.4338	W-RF	0.8234	0.6124	0.5178	W-RF	0.8737	0.7409	0.4674
	LSTM	0.8770	0.7337	0.4295	LSTM	0.9382	0.8549	0.3168	LSTM	0.8796	0.7311	0.4762
	W-LSTM	**0.9836**	**0.9634**	**0.1592**	W-LSTM	0.9518	0.8661	0.3044	W-LSTM	0.9802	0.9452	0.2150
	GPR	0.9387	0.8730	0.2966	GPR	0.9433	0.8831	0.2843	GPR	0.9475	0.8969	0.2948
	W-GPR	0.9794	0.9591	0.1684	**W-GPR**	**0.9811**	**0.9625**	**0.1610**	**W-GPR**	**0.9799**	**0.9603**	**0.1830**

Table 3. *Cont.*

Test Data		Bodø				Karasjok				Oslo		
Model		**r**	**NSE**	**RMSE**		**r**	**NSE**	**RMSE**		**r**	**NSE**	**RMSE**
M02	SVM	0.9409	0.8797	0.2887	SVM	0.9430	0.8847	0.2823	SVM	0.9474	0.8962	0.2959
	W-SVM	0.9939	0.9878	0.0921	**W-SVM**	**0.9946**	**0.9892**	**0.0866**	W-SVM	0.9950	0.9900	0.0919
	RF	0.9095	0.8004	0.3719	RF	0.9188	0.8239	0.3490	RF	0.9261	0.8472	0.3590
	W-RF	0.8688	0.7285	0.4337	W-RF	0.8246	0.6294	0.5063	W-RF	0.8757	0.7515	0.4577
	LSTM	0.9181	0.8234	0.3497	LSTM	0.8869	0.6922	0.4614	LSTM	0.9372	0.8732	0.3271
	W-LSTM	0.9913	0.9766	0.1274	W-LSTM	0.9749	0.9491	0.1876	W-LSTM	0.9217	0.8383	0.3693
	GPR	0.9405	0.8766	0.2924	GPR	0.9428	0.8822	0.2854	GPR	0.9476	0.8970	0.2947
	W-GPR	**0.9939**	**0.9878**	**0.0918**	**W-GPR**	**0.9946**	**0.9892**	**0.0866**	**W-GPR**	**0.9950**	**0.9901**	**0.0916**
M03	SVM	0.9408	0.8794	0.2891	SVM	0.9430	0.8845	0.2827	SVM	0.9475	0.8966	0.2953
	W-SVM	0.9954	0.9909	0.0795	W-SVM	0.9957	0.9913	0.0777	W-SVM	0.9965	0.9929	0.0773
	RF	0.9070	0.7957	0.3762	RF	0.9164	0.8175	0.3553	RF	0.9235	0.8414	0.3657
	W-RF	0.8650	0.7247	0.4367	W-RF	0.8290	0.6455	0.4952	W-RF	0.8745	0.7510	0.4583
	LSTM	0.8533	0.7168	0.4429	LSTM	0.9336	0.8687	0.3014	LSTM	0.8624	0.6877	0.5132
	W-LSTM	0.9723	0.9444	0.1963	W-LSTM	0.9927	0.9854	0.1003	W-LSTM	0.9767	0.9525	0.2002
	GPR	0.9404	0.8765	0.2924	GPR	0.9427	0.8819	0.2859	GPR	0.9477	0.8971	0.2945
	W-GPR	**0.9955**	**0.9909**	**0.0794**	**W-GPR**	**0.9957**	**0.9914**	**0.0769**	**W-GPR**	**0.9968**	**0.9935**	**0.0740**
M04	SVM	0.9408	0.8791	0.2894	SVM	0.9423	0.8832	0.2833	SVM	0.9476	0.8966	0.2953
	W-SVM	**0.9970**	**0.9939**	**0.0648**	W-SVM	0.9979	0.9957	0.0542	W-SVM	0.9977	0.9954	0.0624
	RF	0.9140	0.8146	0.3584	RF	0.9175	0.8213	0.3506	RF	0.9256	0.8497	0.3560
	W-RF	0.8647	0.7241	0.4371	W-RF	0.8329	0.6511	0.4898	W-RF	0.8698	0.7459	0.4629
	LSTM	0.9312	0.8644	0.3065	LSTM	0.8936	0.7279	0.4325	LSTM	0.9304	0.8653	0.3370
	W-LSTM	0.9623	0.8746	0.2947	W-LSTM	0.9726	0.9437	0.1967	W-LSTM	0.7380	0.5416	0.6217
	GPR	0.9405	0.8767	0.2922	GPR	0.9420	0.8801	0.2872	GPR	0.9478	0.8974	0.2941
	W-GPR	0.9969	0.9938	0.0657	**W-GPR**	**0.9981**	**0.9962**	**0.0509**	**W-GPR**	**0.9983**	**0.9966**	**0.0539**
Test Data		**Tromsø**				**Trondheim**				**Vadsø**		
Model		**r**	**NSE**	**RMSE**		**r**	**NSE**	**RMSE**		**r**	**NSE**	**RMSE**
M01	SVM	0.9461	0.8838	0.2742	SVM	0.9400	0.8808	0.3431	SVM	0.9420	0.8760	0.2509
	W-SVM	0.9786	0.9576	0.1655	W-SVM	0.9779	0.9561	0.2081	W-SVM	0.9789	0.9582	0.1457
	RF	0.9089	0.7773	0.3796	RF	0.9055	0.7912	0.4541	RF	0.8979	0.7386	0.3642
	W-RF	0.8472	0.6631	0.4669	W-RF	0.8618	0.7030	0.5416	W-RF	0.8429	0.5703	0.4670
	LSTM	0.9194	0.7554	0.3978	LSTM	0.9350	0.8736	0.3533	LSTM	0.9383	0.8700	0.2568
	W-LSTM	0.9710	0.9393	0.1981	**W-LSTM**	**0.9894**	**0.9789**	**0.1443**	W-LSTM	0.9821	0.9491	0.1607
	GPR	0.9456	0.8834	0.2746	GPR	0.9382	0.8783	0.3467	GPR	0.9419	0.8779	0.2490
	W-GPR	**0.9791**	**0.9587**	**0.1635**	W-GPR	0.9792	0.9589	0.2016	**W-GPR**	**0.9792**	**0.9588**	**0.1447**
M02	SVM	0.9458	0.8829	0.2752	SVM	0.9409	0.8829	0.3401	SVM	0.9413	0.8760	0.2509
	W-SVM	0.9947	0.9893	0.0833	W-SVM	0.9943	0.9886	0.1060	W-SVM	0.9932	0.9863	0.0835
	RF	0.9169	0.8018	0.3581	RF	0.9051	0.7973	0.4474	RF	0.9021	0.7521	0.3547
	W-RF	0.8491	0.6705	0.4617	W-RF	0.8705	0.7225	0.5235	W-RF	0.8371	0.6195	0.4395
	LSTM	0.9188	0.8421	0.3196	LSTM	0.9383	0.8732	0.3539	LSTM	0.9224	0.8486	0.2772
	W-LSTM	0.9799	0.9589	0.1630	W-LSTM	0.9643	0.8996	0.3150	W-LSTM	0.9912	0.9402	0.1742
	GPR	0.9460	0.8847	0.2731	GPR	0.9404	0.8828	0.3402	GPR	0.9413	0.8768	0.2501
	W-GPR	**0.9947**	**0.9895**	**0.0825**	**W-GPR**	**0.9945**	**0.9891**	**0.1039**	**W-GPR**	**0.9933**	**0.9865**	**0.0828**
M03	SVM	0.9457	0.8825	0.2757	SVM	0.9407	0.8826	0.3406	SVM	0.9415	0.8755	0.2514
	W-SVM	0.9954	0.9908	0.0772	W-SVM	0.9950	0.9900	0.0993	W-SVM	0.9951	0.9900	0.0713
	RF	0.9142	0.7907	0.3680	RF	0.9043	0.7974	0.4473	RF	0.9000	0.7367	0.3656
	W-RF	0.8414	0.6471	0.4778	W-RF	0.8718	0.7308	0.5156	W-RF	0.8333	0.6286	0.4342
	LSTM	0.9003	0.7159	0.4287	LSTM	0.9356	0.8675	0.3618	LSTM	0.9088	0.8249	0.2981
	W-LSTM	0.9099	0.8114	0.3493	W-LSTM	0.9870	0.9730	0.1634	W-LSTM	0.9477	0.8897	0.2366
	GPR	0.9457	0.8839	0.2740	GPR	0.9404	0.8828	0.3402	GPR	0.9414	0.8766	0.2502
	W-GPR	**0.9957**	**0.9913**	**0.0749**	**W-GPR**	**0.9955**	**0.9909**	**0.0946**	**W-GPR**	**0.9951**	**0.9902**	**0.0705**

Table 3. *Cont.*

Test Data		Tromsø				Trondheim				Vadsø		
Model		**r**	**NSE**	**RMSE**		**r**	**NSE**	**RMSE**		**r**	**NSE**	**RMSE**
M04	SVM	0.9457	0.8816	0.2768	SVM	0.9402	0.8814	0.3423	SVM	0.9412	0.8785	0.2484
	W-SVM	0.9964	0.9927	0.0688	W-SVM	0.9970	0.9940	0.0768	W-SVM	0.9968	0.9937	0.0568
	RF	0.9227	0.8185	0.3427	RF	0.9109	0.8201	0.4215	RF	0.9018	0.7529	0.3542
	W-RF	0.8437	0.6460	0.4785	W-RF	0.8750	0.7338	0.5128	W-RF	0.8357	0.6336	0.4313
	LSTM	0.9425	0.8792	0.2795	LSTM	0.8518	0.7152	0.5303	LSTM	0.9160	0.8219	0.3006
	W-LSTM	0.9901	0.9739	0.1299	W-LSTM	0.9779	0.9512	0.2196	W-LSTM	0.9618	0.8940	0.2319
	GPR	0.9455	0.8835	0.2745	GPR	0.9400	0.8820	0.3414	GPR	0.9413	0.8763	0.2506
	W-GPR	**0.9965**	**0.9929**	**0.0676**	**W-GPR**	**0.9971**	**0.9942**	**0.0754**	**W-GPR**	**0.9973**	**0.9946**	**0.0524**

Upon examining Table 3, it is evident that the SVM with WT, namely W-SVM, demonstrates the highest performance metrics, r: 0.9970, NSE: 0.9939, and RMSE: 0.0648, in M04 for Bodø, achieving superior performance compared to other models and algorithms. Another notable finding is derived from the GPR with WT, W-GPR. The performance metrics of this model are r: 0.9969, NSE: 0.9938, and 0.0657, showcasing the close correlation of the performance of these two models. This similarity in performance highlights the ability of two models in drought prediction in this region. Further analysis revealed that WT of GPR, W-GPR also performs well with the M03 model, with r: 0.9955, NSE: 0.9909, and RMSE:0.0794, slightly less effective than W-SVM in M04. Given its consistent efficacy in both M04 and M03, GPR with WT, W-GPR, emerges as a successful algorithm in drought analysis conducted for Bodø.

Moreover, an important finding can be observed when the model input structures are examined. There is a 1-month lagged SPEI difference between M04 and M03 and this lagged value positively affected the model performance. While W-GPR yielded successful outcomes in M02, its performance is weaker compared to the M03 and M04 models. In the M01 model, one of the most successful results was obtained with LSTM with WT, namely W-LSTM, with r: 0.9836, NSE: 0.9634, and RMSE: 0.1592. Despite exhibiting satisfactory results, it falls behind the top performer models, which are both M04 and M03, in terms of overall performance. In general, the most successful algorithms for Bodø were obtained with models coupled with WT.

Significant improvements were identified for most of the models with WT, with exceptions for the RF model. For instance, the most successful model for Bodø is W-GPR in M04. The performance metrics of this model prior to WT were r: 0.9405, NSE: 0.8767, and RMSE: 0.2922, whereas the metrics after WT were r: 0.9970, NSE: 0.9939, and RMSE: 0.0648, showing an impressive improvement. Due to its accuracy and effectiveness, W-SVM in M04 should be the preferred model for drought modeling in Bodø. In addition, W-GPR in M04 can be preferred as an alternative due to its similar performance. The time series of the two most effective models, W-GPR and W-SVM in M04, for this region were illustrated in Figure 4. In the analyses performed without WT, the most effective result for this region was obtained in M01 with SVM.

Considering Figure 4, a striking observation is the strong agreement between observed and predicted values of the models. Both models appear to follow a single line and capture all the peak points, which clearly indicates both models were determined to be successful for drought prediction in this region.

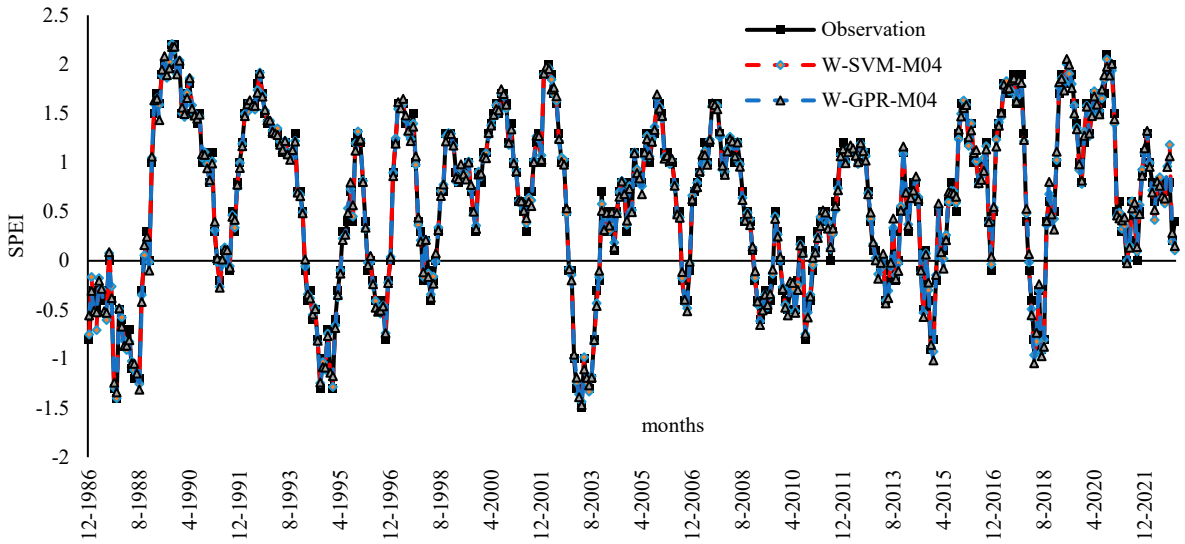

Figure 4. The most successful two models for Bodø with *W-SVM-M04* analysis of SVM with WT in M04 and *W-GPR-M04* analysis of GPR with WT in M04.

Moving on to the Karasjok region, the performance metrics exhibit slightly better results compared to those obtained in Bodø. Similar to Bodø, the most impressive performance results were obtained in M04 by utilizing W-GPR, with r: 0.9981, NSE: 0.9962, and RMSE: 0.0509. This model is followed by W-SVM in M04 in terms of performance, which achieved r: 0.9979, NSE: 0.9957, and RMSE: 0.0542, demonstrating a close performance to W-GPR. Although the performance values of W-GPR and W-SVM are very close to each other, as in Bodø, W-GPR represent slightly better results compared to W-SVM in this region. It can be concluded that both W-GPR and W-SVM consistently deliver the most effective prediction results. M02 further supports the above conclusion, with identical performance metrics in W-SVM M02 and W-GPR M02, with r: 0.9946, NSE: 0.9892, and RMSE: 0.0866. In M01 and M03 models, the most effective results were obtained with W-GPR; however, these performance values were lower than that determined in M04. The findings obtained from the analyses conducted for Karasjok indicate that the highest performance values were achieved using W-GPR in M04 and the performance metrics of all algorithms improved after WT, aside from RF, which showed a decrease. Prior to WT, analyses revealed that the most desirable results for this region were observed in M01 using SVM, with r: 0.9433, NSE: 0.8850, and RMSE: 0.2820.

Figure 5 visually illustrates the difference in performances between observed and predicted model drought values achieved by the best two models, W-SVM-M04 and W-GPR-M04, in time series analysis. Overall, no difference was observed and a remarkable agreement revealed between observed and predicted values. Both prediction models provide a good representation of the peak points and demonstrate the ability to accurately capture the drought in the region.

In the Oslo region, the results obtained from the analyses reveal that W-GPR on the M04 model achieved the highest performance with r: 0.9983, NSE: 0.9966, and RMSE: 0.0539. Another algorithm that achieved successful results in M04 models is W-SVM, with r: 0.9977, NSE: 0.9954, and RMSE: 0.0624. The input structure of the M04 model was created from SPEI data of lagged times t-1, t-2, t-3, t-4, t-11, t-13, and t-12. The M03 model follows these top performer models in terms of performance with r: 0.9968, NSE: 0.9935, and RMSE: 0.0740 values. The difference in the input structure of the M04 and M03 models is the inclusion of a 1-month lagged SPEI value. By including this variable into the models, the performances of the models were enhanced, showing the importance of model accuracy in prediction. Furthermore, it is noteworthy that W-GPR outperforms other algorithms in all models (M01, M02, M03, and M04) in the Oslo region. W-SVM lagged behind W-GPR in terms of performance in all models, M01, M02, M03, and M04. The common point of these

models is the application of WT to increase model performance. In the analysis, without WT, the most successful performance value achieved with GPR in M04 with r: 0.9478, NSE: 0.8974, and RMSE: 0.2941. Despite this, GPR performed better than other algorithms, both with WT and without WT in analyses for this region. Hence, this approach is recommended for implementation in a drought modeling activity to be carried out in this area. Another point that should be mentioned here is the adverse effect of WT on the performance of the RF model. This observation is consistent across all investigated regions, suggesting that inclusion of WT may not be suitable for enhancing the model performance every time.

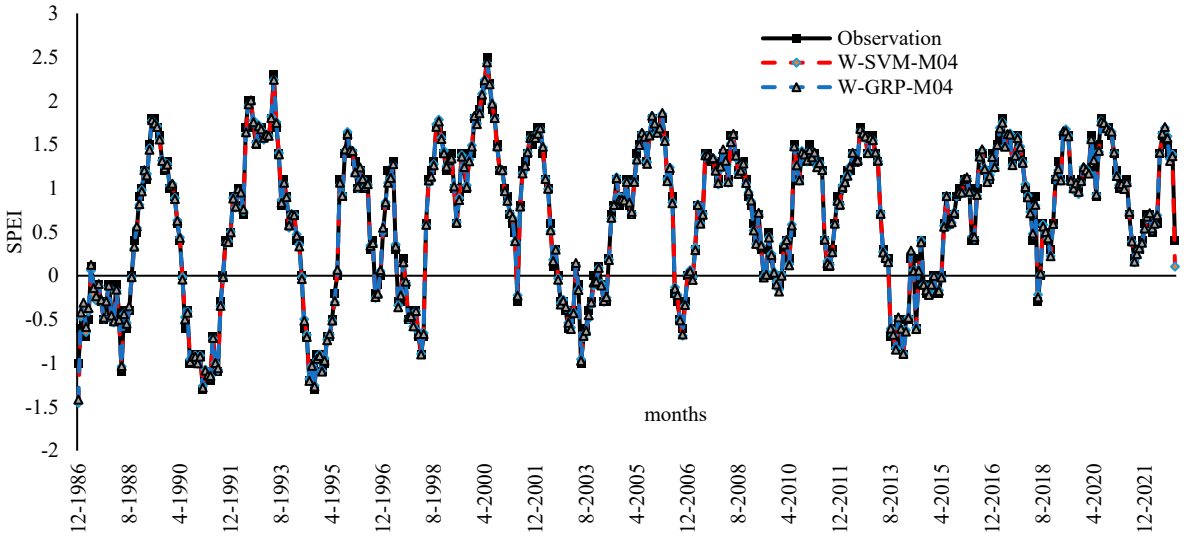

Figure 5. The most successful two models for Karasjok with *W-SVM-M04* analysis of SVM with WT in M04 and *W-GPR-M04* analysis of GPR with WT in M04.

The time series of observation values and prediction values of W-GPR-M04 and W-SVM-M04, which were determined to be the most successful models for Oslo, are shown in Figure 6. According to this figure, it was determined that both methods were compatible with the observation values and the peak points were captured successfully by the models.

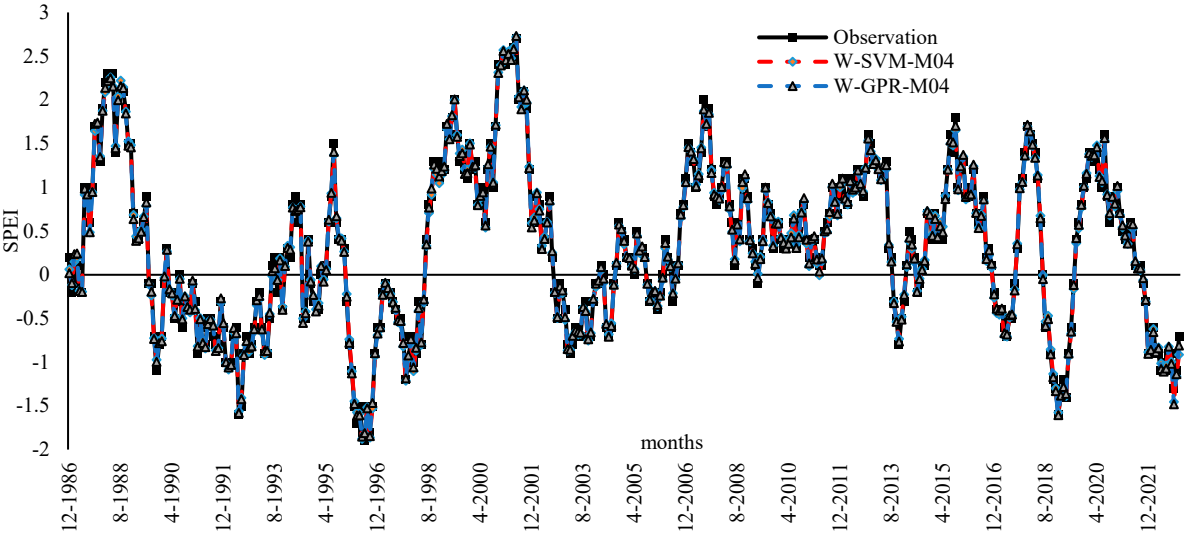

Figure 6. The most successful two models for Oslo with *W-SVM-M04* analysis of SVM with WT in M04 and *W-GPR-M04* analysis of GPR with WT in M04.

In the Tromsø Region, the W-GPR-M04 model emerged as the most successful algorithm, with remarkable performance metrics, with r: 0.9965, NSE: 0.9929, and RMSE:

0.0676 values obtained. Similar to the findings in Oslo, W-SVM-M04 also achieved comparable performance metrics with r: 0.9964, NSE: 0.9927, and RMSE: 0.0688. However, ultimately it cannot surpass the effectiveness of W-GPR-M04. In the M03 model, W-GPR also showed strong performance with r: 0.9957, NSE: 0.9913, and RMSE: 0.0749. Considering M03, while the performance of W-SVM ranked higher than other techniques, it lagged behind W-GPR. The lowest performance values in this class were observed for W-RF, with r: 0.8414, NSE: 0.6471, and NSE: 0.4778. A notable observation in Tromsø is that the performance metrics of GPR without WT surpassed those of other techniques. Regardless of the application of WT, GPR can be assumed to be the effective algorithm that can capture the drought patterns in the region. Thus, for Tromsø, it is advisable to consider both GPR with WT and without WT. When it comes to M02, the most successful performance is obtained with W-GPR, achieving r: 0.9947, NSE: 0.9895, and RMSE: 0.0825. While these metrics are comparable to the performance of M03 and M04, they are comparatively lower, which suggests a slightly lower performance for W-GPR in M02. In the M01 model, the W-GPR again delivered the most successful results with r: 0.9791, NSE: 0.9587, and RMSE: 0.1635. Similar to previous models, the most effective outcomes in this category were achieved with GPR using WT. In the analysis without WT, SVM showed effective performance compared to other models in this class. M01, M02, M03, and M04 used as models in Tromsø were designed to include various data formats. One further outcome in this context is that the input structure of M04 was generally more successful with WT than other algorithms. In every analysis performed with WT, it has been determined that GPR consistently performed effectively across all algorithms.

In the analysis conducted for the Tromsø region, W-GPR-M04 and W-SVM-M04 demonstrated more successful results compared to other models and algorithms. To further understand the performance and the predictive capabilities of these models, their time series are visualized in Figure 7.

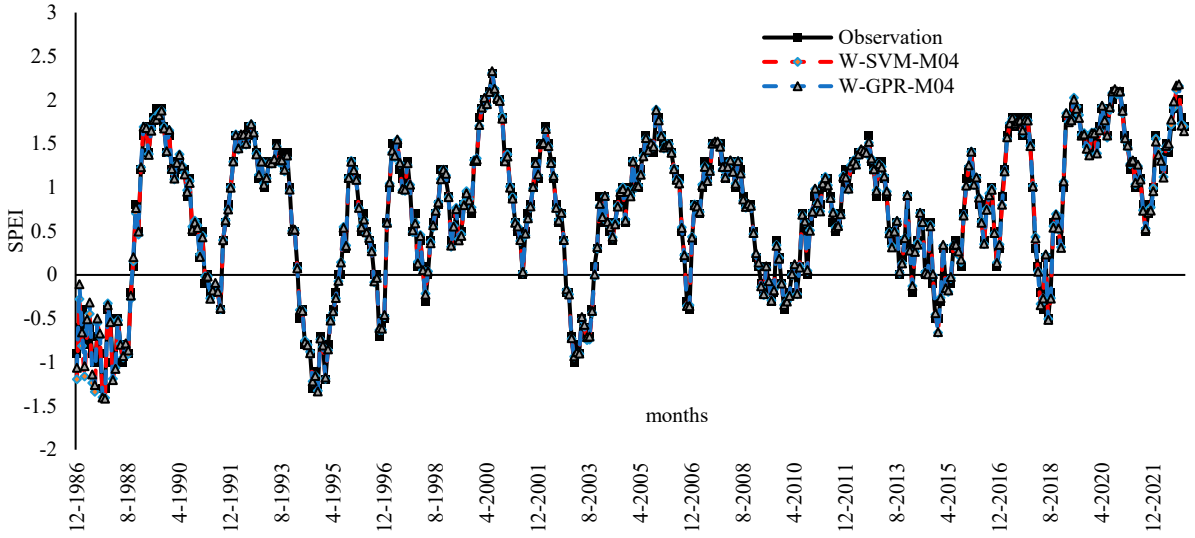

Figure 7. The most successful two models for Tromsø with *W-SVM-M04* analysis of SVM with WT in M04 and *W-GPR-M04* analysis of GPR with WT in M04.

Figure 7 demonstrates the remarkable agreement between the observed drought values and the predictions from the two most effective models, namely W-SVM and W-GPR for M04 model. Both models accurately captured the observed drought patterns, showcasing their ability to predict drought conditions in Tromsø.

The Trondheim area was analyzed using four distinct models and approaches, both with and without WT. Based on the findings of this analyses, the most effective model was identified as the W-GPR in M04, with r: 0.9971, NSE: 0.9942, and RMSE: 0.0754. In M04, the W-SVM model closely followed this model in terms of performance, with r: 0.9970,

NSE: 0.9940, and RMSE: 0.0768. While the performance metrics of these two models are almost identical, the W-GPR model slightly outperforms W-SWM and outperforms other models, demonstrating its superiority in predicting drought conditions in Trondheim. All of these presented models were derived using WT. The optimization conducted without WT yielded the optimal outcome in M04, which was again achieved by GPR. Therefore, GPR was determined as the best algorithm in the analyses performed both with and without WT in M04. The best model in M03 was obtained with W-GPR, with r: 0.9955, NSE: 0.9909, and RMSE: 0.0946, indicating slightly lower accuracy compared to the two models with WT mentioned earlier. Furthermore, the analyses using W-SVM revealed the second most effective algorithm in this category with r: 0.9950, NSE: 0.9900, and RMSE: 0.0993. The W-GPR algorithm achieved the highest performance in M02 with r: 0.9945, NSE: 0.9891, and RMSE: 0.1039, while the W-LSTM model emerged as the strongest performer in M01, achieving r: 0.9894, NSE: 0.9789, and RMSE: 0.1443.

The most effective models in simulations conducted without WT are SVM in M02 and M01. The least successful algorithm for this region is W-RF in M01, with r: 0.8618, NSE: 0.7030, and RMSE: 0.5416. It should also be noted that the performance values of this model before WT are better than the results obtained after WT. As a result of the analyses carried out in Trondheim, the two best models obtained among all models are W-GPR-M04 and W-SVM-M04. The time series of observed values with these models is shown in Figure 8.

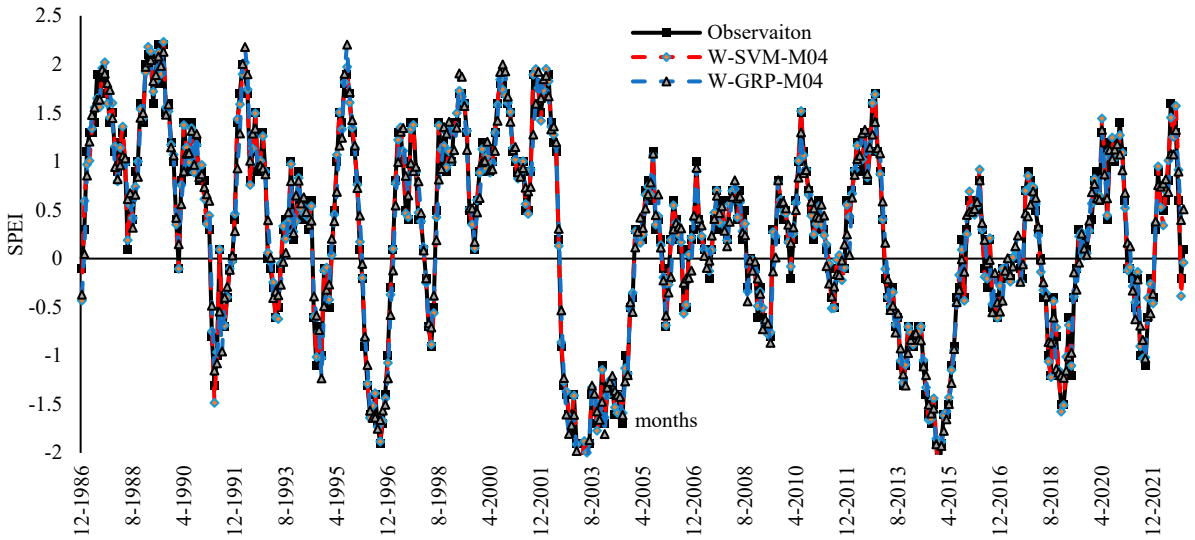

Figure 8. The most successful two models for Trondheim with *W-SVM-M04* analysis of SVM with WT in M04 and *W-GPR-M04* analysis of GPR with WT in M04.

While Figure 8 provides visualization of a good fit between both W-SVM-M04 and W-GPR-M04 and the observed values, it was identified that the W-SVM-M04 model did not accurately capture the peak values in drought time series. Figure 8 clearly demonstrates that W-GPR-M04 outperforms the W-SVM-M04 model in identifying the peak values.

The final region examined is Vadsø. This region yielded findings identical to those observed in other investigated locations. The best performance values for this region were obtained with W-GPR in M04, achieving r: 0.9973, NSE: 0.9946, and RMSE: 0.0524. This model is closely followed by W-SVM with r: 0.9968, NSE: 0.9937, and RMSE: 0.0568. While the performance metrics of these two models differ slightly, W-GPR is often regarded as the most successful model in this region due to its superior r, NSE, and RMSE values compared to the others. The most successful algorithm in this class was obtained with the WT again, yet the SVM model without WT also achieved acceptable performance values with r: 0.9412, NSE: 0.8785, and RMSE: 0.2484 at M04 in the analyses conducted. M04 emerged as the most successful model for this region, with M03 adhering to this model regarding predictive capability. Compared to other models, the W-GPR model achieved

the most optimal performance parameters in M03, with r: 0.9951, NSE: 0.9902, and RMSE: 0.0705. The most effective algorithm, as in most other regions, has been W-GPR in the Vadsø analysis. In M02 and M01 models, the most successful algorithm detected was also W-GPR. The assessed performance metrics for W-GPR in M01 are r: 0.9792, NSE: 0.9588, and RMSE: 0.1447, and in M02, the same metrics are r: 0.9933, RMSE: 0.9865, and RMSE: 0.0828. Additionally, the most successful models for this region were determined by WT. In the analyses performed without WT, the SVM model was found to be the most successful model in M04.

Figure 9 illustrates the correlation between the observed values and the predictions of the two most effective algorithms, W-GPR-M04 and W-SVM-M04, in Vadsø. Similar to the findings in other regions, Figure 9 visualizes the strong agreement between observations and the two models' predictions, indicating that both W-GPR-M04 and W-SVM-M04 effectively capture the drought patterns in Vadsø region, accurately identifying the peak values.

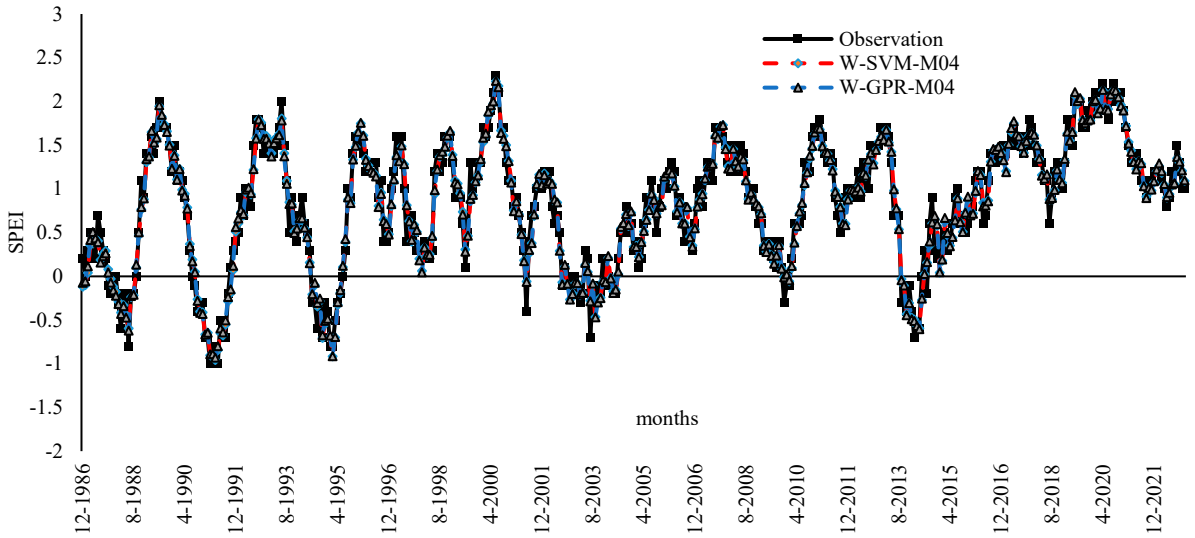

Figure 9. The most successful two models for Vadsø with W-SVM-M04 analysis of SVM with WT in M04 and W-GPR-M04 analysis of GPR with WT in M04.

The table displays the statistical evaluation results for all the study regions. In addition to these tables, several visual comparisons were also made to gain further understanding of model and algorithms' performance. One of these comparisons is the 3D scatter diagram in Figure 10. In this figure, performance of two of the most successful models across six different stations are illustrated. With this diagram, it is possible to determine the best model for each region. Moving towards the right and the bottom sides of the 3D graph, the performance of the models exhibits an improvement, with higher r, NSE, and RMSE values observed. In the Bodø region, best performance was obtained with W-SVM-M04, confirming the statistical results. W-GPR-M03 and W-GPR-M02 closely follow this model in terms of performance. In Karasjok, the W-GPR-M04 model achieved the highest level of success in in the 3D analyses, whereas the SVM-M02 model generated the lowest performance among the models. Statistical findings and 3D graphical interpretations in the Oslo region exhibit a close match. Here, the W-GPR-M04 model accomplished the highest level of success while the RF-M03 model demonstrated the lowest performance among the models. According to Figure 10, the most successful performance in the Tromsø, Trondheim, and Vadsø regions were achieved with W-GPR-M04, in accordance with 3D scatter analysis. W-GPR-M04 consistently demonstrated the highest level of success in terms of overall performance across all regions.

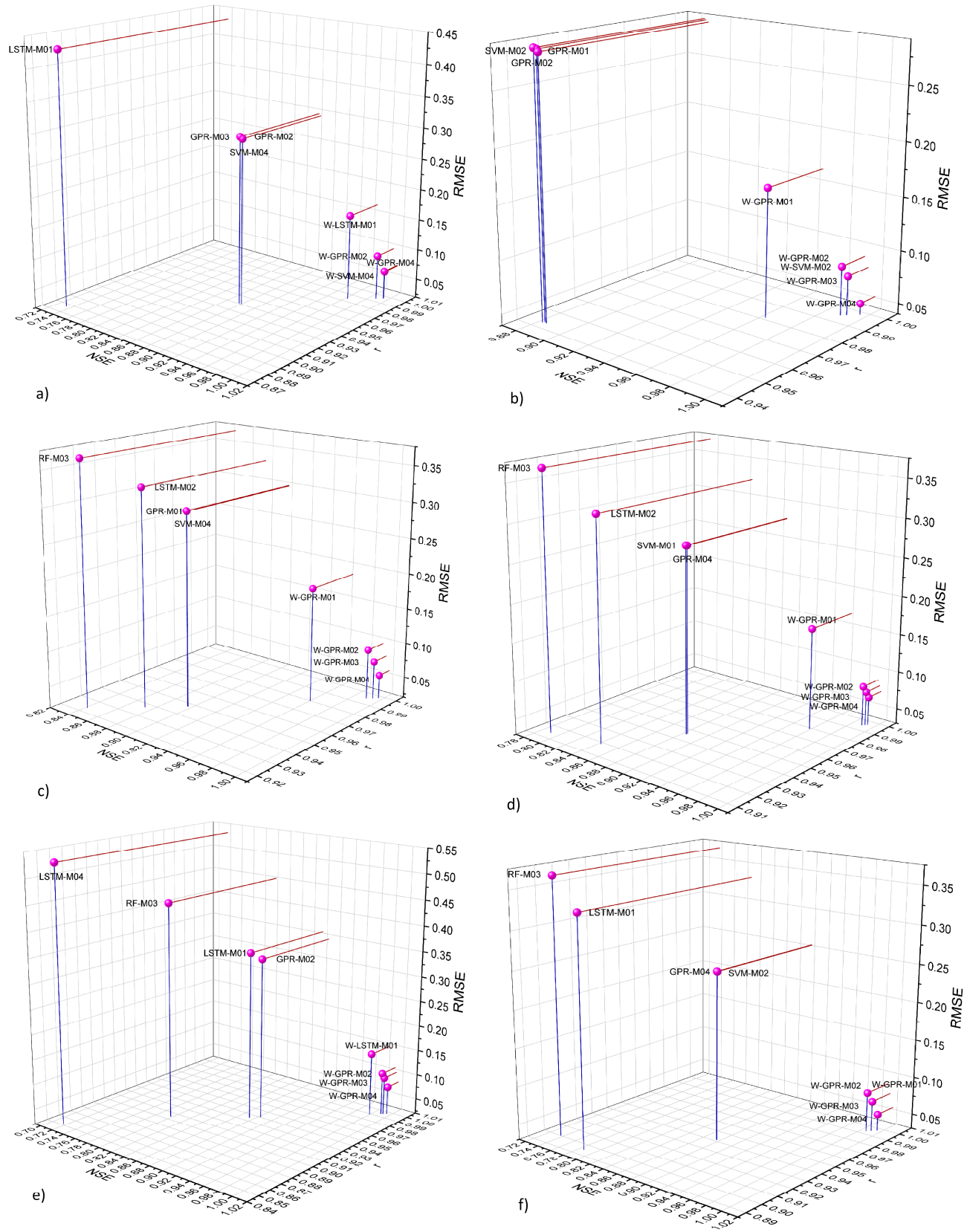

Figure 10. The results on 3D scatter diagram based on study area of (**a**) Bodø, (**b**) Karasjok, (**c**) Oslo, (**d**) Tromsø, (**e**) Trondheim, and (**f**) Vadsø with RF-M03 analysis of RF in M03, W-GPR-M04 analysis of GPR with WT in M04, etc.

The Taylor diagram is a graphical technique used to compare data by means of their RMSE, correlation coefficient, and NSE values. As applied in the 3D scatter analyses strategy, the two most successful models for each area were selected and plotted on the Taylor diagram. Taylor diagram analyses conducted in the Bodø region revealed that the W-SVM-M04 model exhibits a superior level of closeness to the observed value compared to the other models (Figure 11). This high-level agreement indicates the robustness of W-SVM-M04, among others. While the W-GPR-M04 model was the second most successful model in this region, Bodø, in Karasjok, Oslo, Tromsø, Trondheim, and the Vadsø regions, it outperformed W-SVM-M04. According to the Taylor diagram, the most successful algorithm was W-GPR-M04 across all regions, conforming the findings of 3D scatter and statistical results except for Bodø. Both statistical and graphical results largely overlap in this section, stating the consistency of the analyses.

The box normal chart provides another graphical comparison method for model performance evaluation. Here, the normal distribution, mean, and median values of the model data are used and compared against observed values. The box normal chart created using the two most successful models for the study regions are shown in Figure 12. When Figure 12 is examined, it is evident that the average and median values of the observed data in the Bodø region mostly overlap with W-SVM-M04. Therefore, among the compared algorithms, the most successful algorithm for the Bodø region is W-SVM-M04 regarding the drought patterns. Considering the median, mean, and normal distribution, the W-GPR-M04 model demonstrated the best results in all regions except Bodø (Figure 12). The box normal plots also provide a perspective that is consistent with the statistical results, further supporting the overall conclusion.

The violin diagram is a powerful graphical comparison method, providing comprehensive insights into the distribution of model data and the observation. By using violin diagrams, parameters such as first and third quartile, kernel density, mean value, median value, standard deviation, and extreme values can be displayed and compared with observed values. As it is a widely used technique in the literature and provides a detailed model performance view, this study includes large visuals of violin diagrams. As with other graphical methods, Figure 13 presents the comparison of each model with observations separately on a regional basis.

Investigating Figure 13 for the Bodø region, several models are similar in shape compared to the observation values. However, with a closer look at the median, mean, and extreme values, it was determined that W-SVM-M04 was the most successful model, demonstrating the best representation of the observation values. The median and mean values of W-GPR-M04 displayed slightly higher levels than the observation values, making it the second best-performing model in this region. The results here are consistent with the statistical findings, confirming the performance of W-SVM-M04 and the accuracy of W-GPR-M04. An analysis of the violin diagram for Karasjok revealed that the W-GPR-M04 model exhibited a higher degree of resemblance to the observation values than other models, particularly in the third quartile, in terms of the median and mean values. W-SVM-M04 also followed behind the W-GPR-M04 in terms of performance. Another notable result for this region is that SVM-M02 demonstrated the lowest performance among the visually evaluated models in this region. For the Oslo region, the W-GPR-M04 model showed the highest similarity to the observed values, presenting the closest alignment in terms of median, mean, and extreme values. The RF-M03 model had the lowest performance, unlike the competing algorithms. Finally, analysis of the violin diagrams for Tromsø, Trondheim, and Vadsø revealed that the W-GPR-M04 model was the most successful, while the RF-M03 model exhibited the lowest performance based on the median, mean, and extreme values. The insights derived from the violin diagram align with the statistical results derived previously for the study regions.

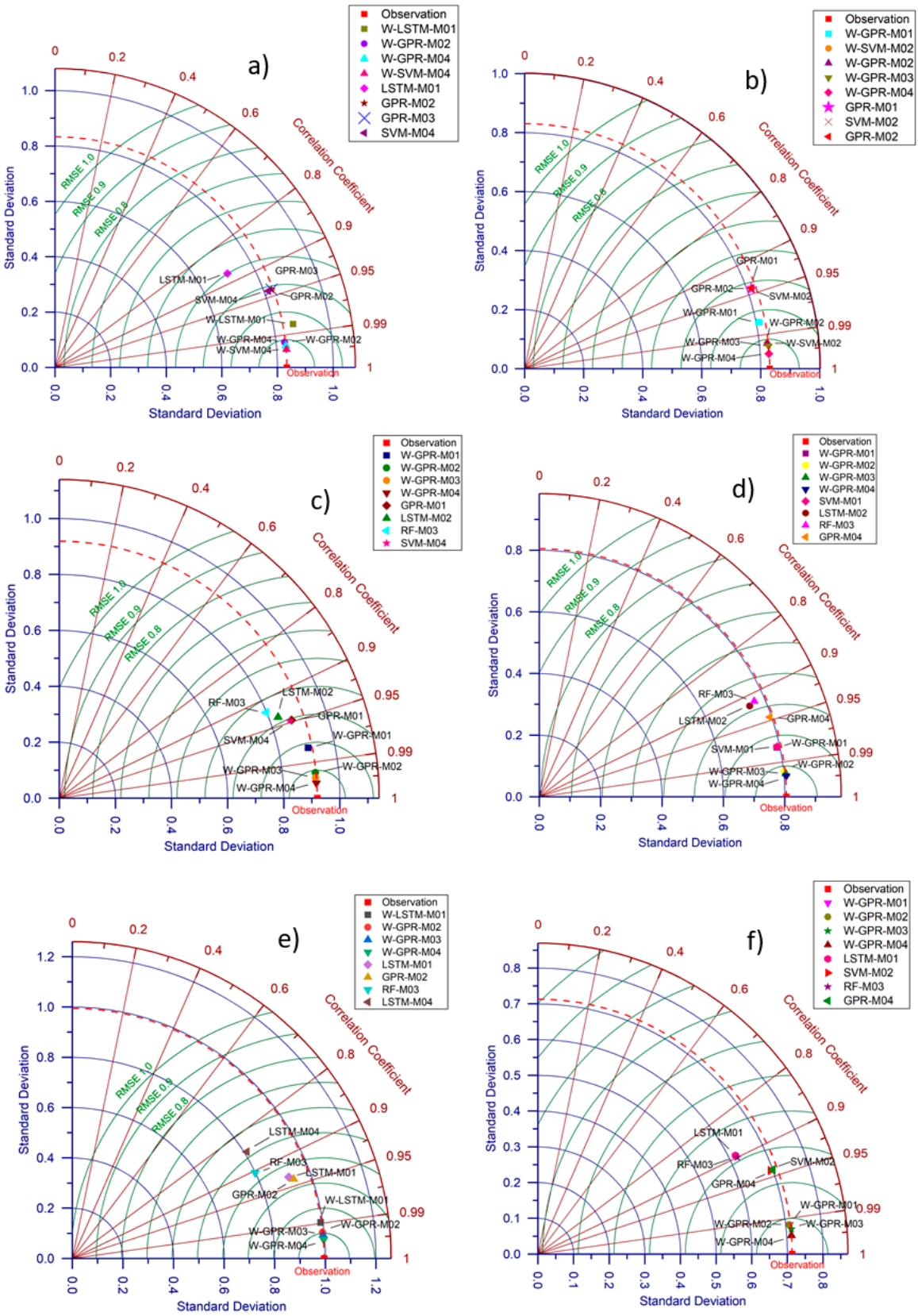

Figure 11. The results of the Taylor diagram based on the study area of (**a**) Bodø, (**b**) Karasjok, (**c**) Oslo, (**d**) Tromsø, (**e**) Trondheim, and (**f**) Vadsø with RF-M03 analysis of RF in M03, W-GPR-M04 analysis of GPR with WT in M04, etc.

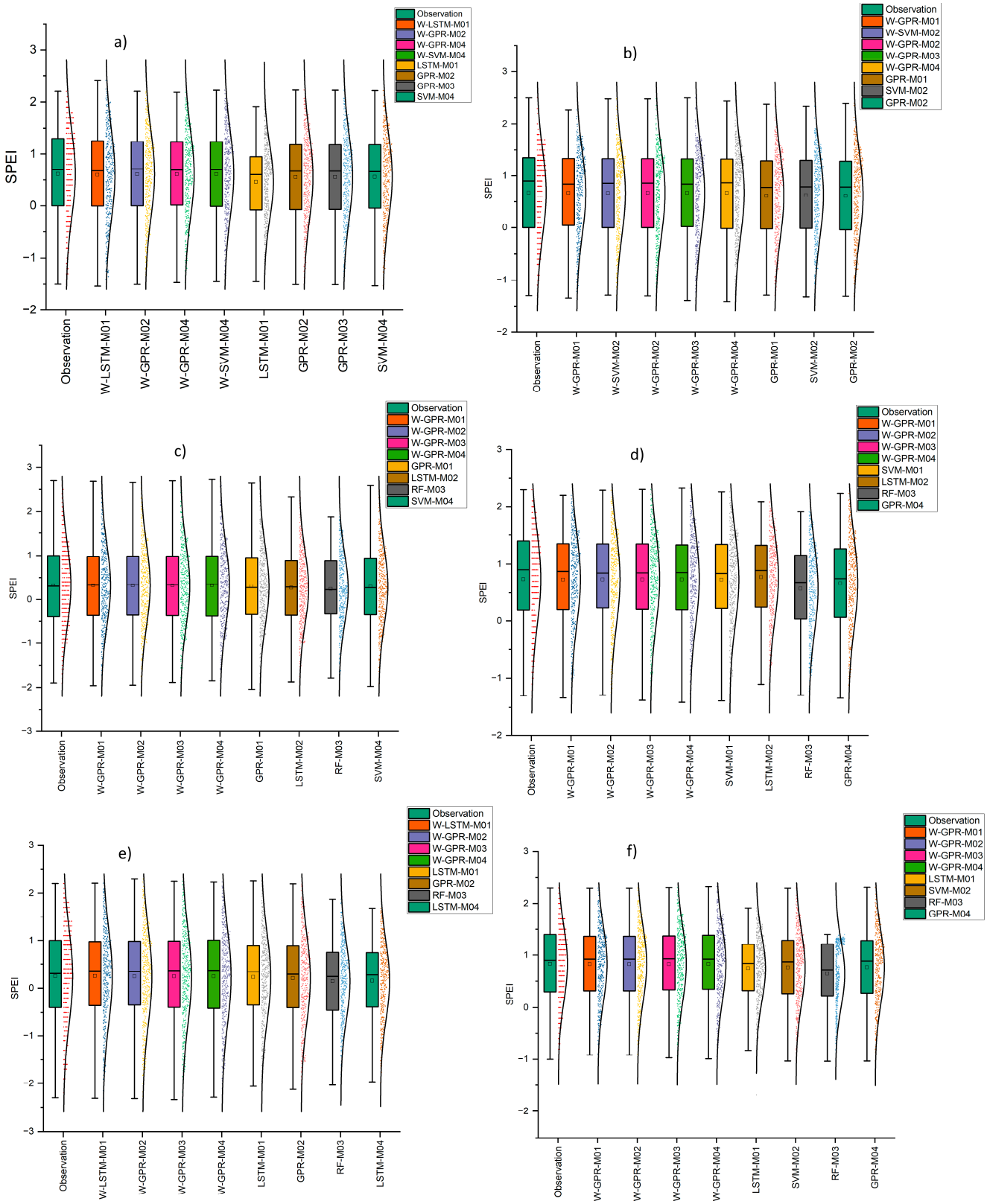

Figure 12. The results of box normal diagram based on study area of (**a**) Bodø, (**b**) Karasjok, (**c**) Oslo, (**d**) Tromsø, (**e**) Trondheim, and (**f**) Vadsø with RF-M03 analysis of RF in M03, W-GPR-M04 analysis of GPR with WT in M04, etc.

RSR is a statistical and visual approach used to evaluate the performance of algorithms on a region-by-region basis. Table 4 presents the rating of model performance according to the RSR value. In this study, the RSR was employed to enrich the visual and statistical interpretation of the results. Figure 14 illustrates the RSR values for each different region. One key highlight from the RSR is that W-SVM and W-GPR generally demonstrate very close performance results. However, it has been determined that W-GPR consistently outperforms W-SVM in terms of performance across all regions. Another notable finding is that, when all regions were compared, the lowest RSR was found in Vadsø (W-GPR), while the most successful result in statistical evaluation suggested the highest success in Oslo (W-GPR). This result shows that the most successful modeling results were determined for Vadsø and indicate the importance of considering specific characteristics of the regions when evaluating drought prediction models.

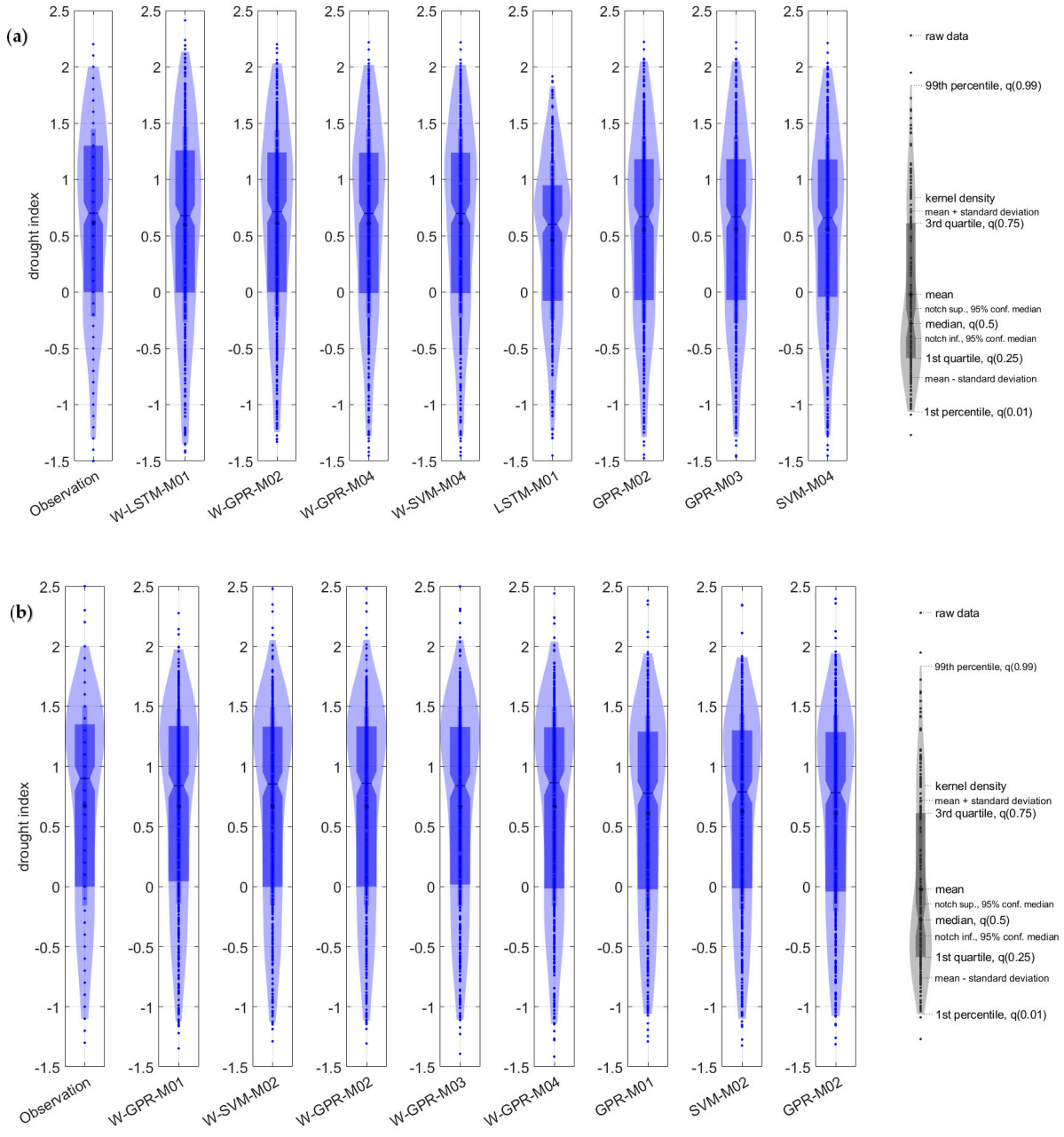

Figure 13. *Cont.*

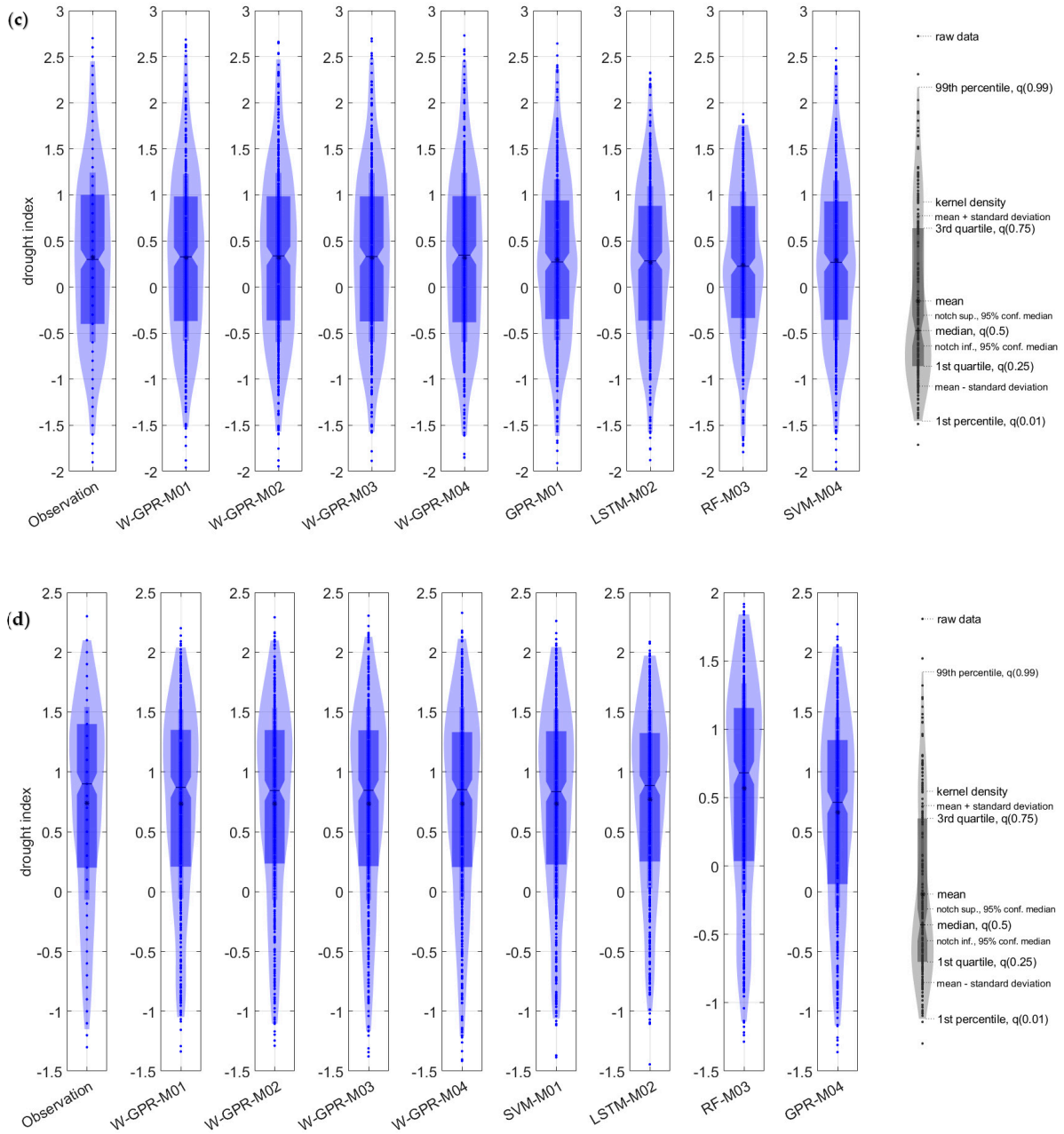

Figure 13. *Cont.*

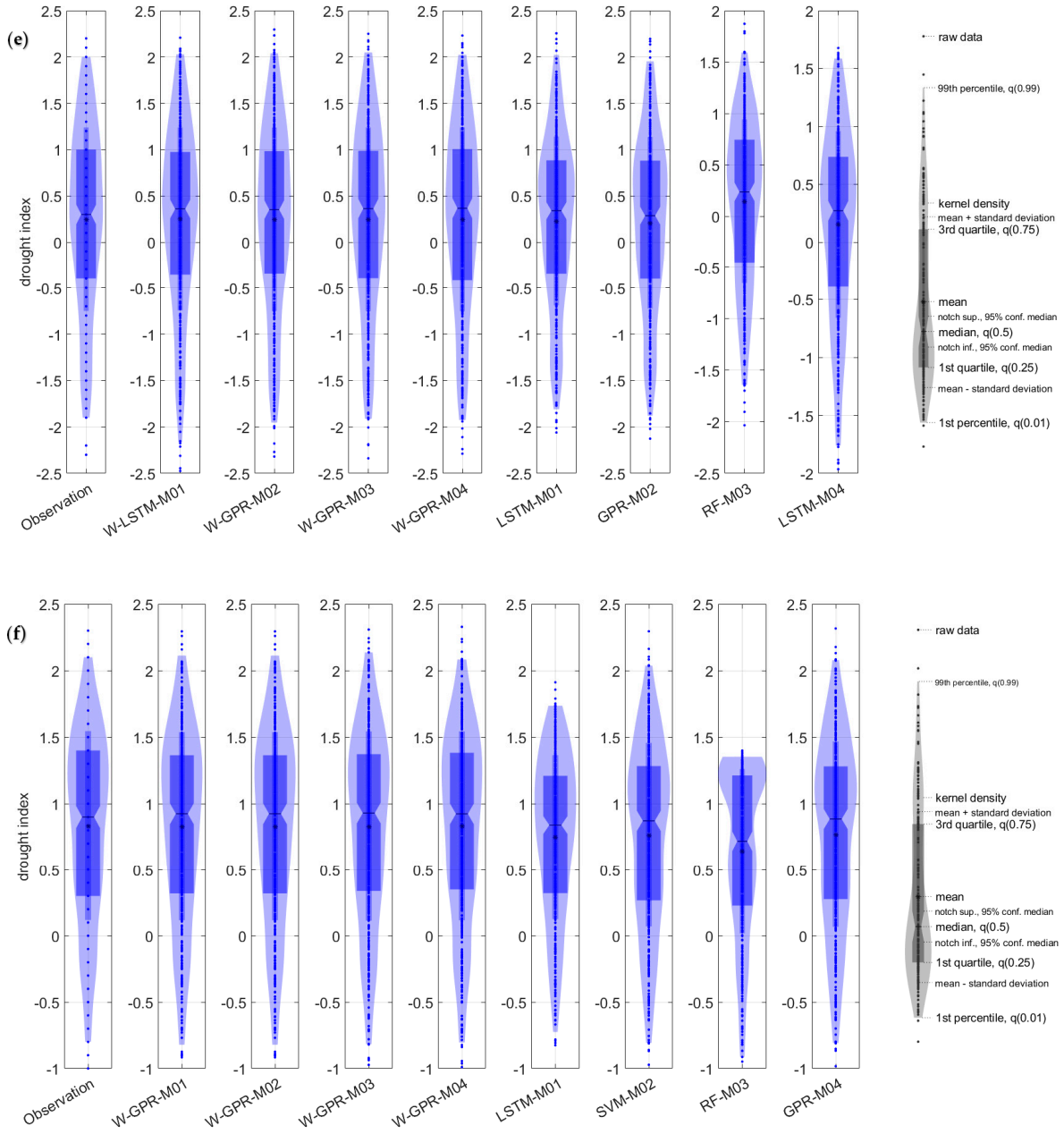

Figure 13. The results on a violin diagram based on the study area of (**a**) Bodø, (**b**) Karasjok, (**c**) Oslo, (**d**) Tromsø, (**e**) Trondheim, and (**f**) Vadsø with RF-M03 analysis of RF in M03, W-GPR-M04 analysis of GPR with WT in M04, etc.

Table 4. RSR range and the corresponding performance rate.

Performance Rating	Unsatisfactory	Satisfactory	Good	Very Good
RSR value	RSR $\geq$ 0.7	0.7 > RSR $\geq$ 0.6	0.6 > RSR $\geq$ 0.5	0.5 $\geq$ RSR

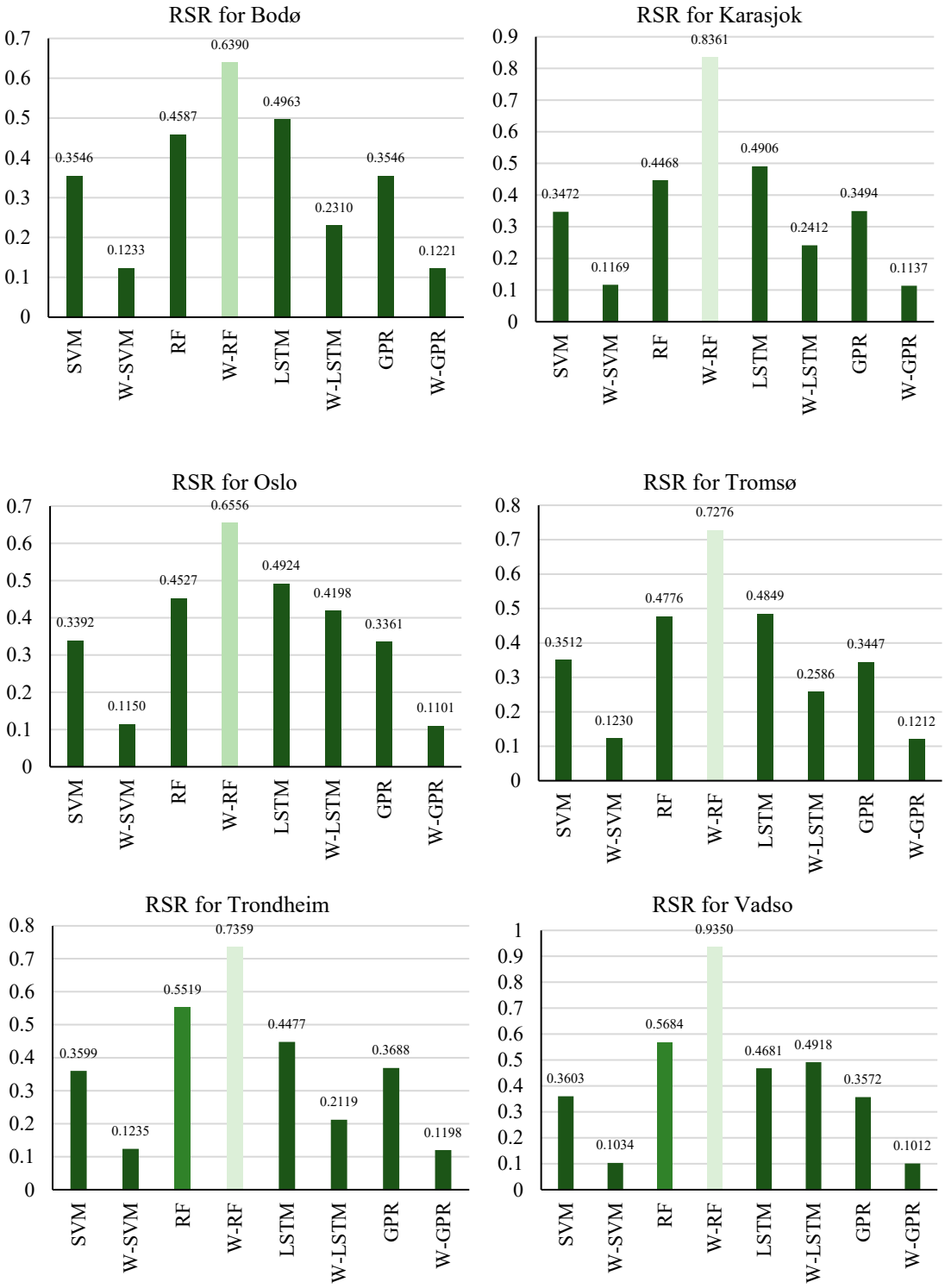

Figure 14. RSR value for all regions (where each color means Unsatisfactory , Satisfactory , Good , Very Good).

In this study, drought modeling using SVM, RF, LSTM, and GPR methods was investigated for six different regions in Norway. WT was also incorporated to enhance model performance. Four distinct model types were employed in drought simulations, with SPEI12 values lagged at various time intervals as input data. In total, 70% of the input data were used for learning and 30% for testing, respectively. Several researchers conducted drought modeling studies using the similar methodologies to this study, with findings that

generally support ours. For instance, Ghasemi et al. [73] developed drought prediction models with three different machine learning algorithms, GPR, general regression neural network (GRNN), and MLP by using SPEI12 in the Iranian region. They reported that the GPR model achieved the lowest RMSE and the highest R^2 values. In this study, the most successful algorithm was also found to be GPR with WT for drought prediction. Additionally, in analyses performed without WT, GPR was the most successful algorithm in some regions, such as Oslo in M04. Another relevant study, by Tuğrul and Hinis [16], who conducted drought modeling using RF, SVM, decision tree (DT), and ANN for the Apa Dam region. They utilized different time-steps of SPI and applied WT to enhance model performance. They stated that SVM with WT was better than other methods and that WT can negatively impact the performance of the RF algorithm. In this study, the WT of RF negatively affected the mode result.

Citakoglu and Coşkun [100] conducted a study on drought forecasting using a set of machine learning algorithms, GPR, ANN, and ANFIS, with meteorological data between 1960 and 2020 in Sakarya. They also employed WT, including variation mode decomposition (VMD), and empirical mode decomposition (EMD) to improve the model performance. They concluded that the hybrid GPR model outperformed other methods as in this study. Another study with similar results is that of Karbasi et al. [101], who investigated drought in Iran using GPR, MLP, and the cascade neural network (cascade-NN) algorithms and enhanced the model outcomes using WT. They concluded that W-GPR demonstrated superior performance in comparison with the alternative approaches mentioned in their study. According to this study, significant outcomes were observed with LSTM prior to WT in some areas. The LSTM model has proven to be an effective prediction tool for those locations. Several studies have also shown that LSTM is an effective prediction tool, such as Wang et al. [35], Taylan [38], and Poornima and Pushpalatha [102].

Considering drought forecasting, there are studies that utilized various techniques, yet this study differs with several aspects. For instance, Elbeltagi et al. [42] initially computed the SPI6 and SPI12, incorporating rainfall data from 1990 to 2019 in the Upper Godavari River basin region. Subsequently, they developed ten distinct models and examined them pairing GPR, RF, and RT algorithms for drought forecasting. The authors concluded that RF yields superior outcomes compared to alternative approaches. In contrast to this study, the best results were obtained by GPR and SVM without WT. This variation underlines the complexity of drought patterns and the importance of regional characteristics, and the data employed.

4. Conclusions

This study developed and evaluated drought prediction models for six locations in Norway by utilizing SPEI data. SVM, LSTM, GPR, and RF, models were implemented, and the model findings were further enhanced using WT. Inclusive of both statistical and graphical representations, this study yielded in-depth findings:

Post-WT, SVM and GPR demonstrated comparable outcomes. Nevertheless, GPR yields the most favorable outcomes.

- While improvements were detected in all algorithms after WT, it led to performance decrease in RF. In addition, RF exhibited the weakest overall performance among the others.
- The M04 model structure usually was the most successful across various techniques and regions. The model structure yielded favorable robustness and suitability for all analyzed locations.
- For the Oslo region, the GPR method, particularly with the M04 structure with and without WT, emerged as the optimal choice for the drought modeling research.
- Analyses conducted throughout Norway revealed the greatest performance values for Oslo compared to other regions, particularly when the W-GPR-M04 model was utilized.

- For potential drought studies, the W-GPR-M04 model structure is recommended in Karasjok, Oslo, Tromsø, Trondheim, and Vadsø, while W-SVM-M04 is suggested for Bodø based on their superior performance with WT.
- Prior to WT implementation, SVM-M01 (Tromsø, Karasjok, and Bodø), GPR-M04 (Oslo), GPR-M02 and GPR-M03 (Trondheim), and GPR-M02 (Vadsø) showed the most favorable performance, highlighting possible sensitivities to WT.
- Based on the RSR values, Vadsø showed the most successful overall performance.
- Among the graphical outputs, Taylor and violin diagrams consistently provided the most comprehensive and reliable insights.
- As previously mentioned, WT generally has a positive effect except when used with RF. The most significant and proportionally best improvement from using WT was achieved in the Oslo region with the LSTM algorithm.
- Earlier sections have demonstrated that the most effective model input structure is M04. The conclusion drawn is that increasing the number of parameters influencing the model correlates with enhanced model performance.
- GPR with WT produced effective outcomes across all locations. Examination of Bodo showed that SVM with WT is more effective compared to other algorithms. Notably, Bodo is located in a coastal area. These findings indicate that both GPR with WT and SVM with WT yield effective results in coastal regions.
- In the analysis of LSTM with WT in the Oslo region, the performance metrics for M04 before applying WT were better than those after applying WT. It was concluded that this algorithm was not effective in the Oslo region.

The research findings provide valuable insights, particularly in the context of climate change, in Norway. The outcomes of this study offer enhanced understanding of water resource management, risks associated with drought, and also guide water-related institutions and organizations.

Considering Norway's vulnerability to higher-than-average temperatures as a result of climate change, several recommendations for future research emerge:

It is thought that this study will help the relevant people in water resources management in the region and the decision-making authorities on these issues. If it is carried out in future projects, risk assessments, or a study on drought prevention, this study should be used.

1. Exploring the use of alternative drought indices beyond SPEI.
2. Expanding the network of meteorological stations in the region to enhance data availability and support more comprehensive drought modeling efforts.
3. Incorporating a wider range of model input variables, such as sea level and sea surface temperature, to capture potential influences on drought dynamics.

Author Contributions: Conceptualization was conducted by M.A.H. and S.O.; methodology was conducted by M.A.H., S.O. and T.T.; writing—review and editing was conducted by M.A.H., S.O. and T.T.; visualization was conducted by M.A.H., S.O. and T.T.; and supervision was conducted by M.A.H. and S.O. All authors have read and agreed to the published version of the manuscript.

Funding: This research received no external funding. APC is supported by UiT the Arctic University of Norway.

Data Availability Statement: The original contributions presented in the study are included in the article. The raw data supporting the conclusions of this article will be made available by the authors upon reasonable request.

Conflicts of Interest: The authors declare that they have no known competing financial interests or personal relationships that could have appeared to influence the work reported in this paper.

References

1. IPCC. *2023: Climate Change 2023: Synthesis Report. Contribution of Working Groups I, II and III to the Sixth Assessment Report of the Intergovernmental Panel on Climate Change*; Core Writing Team, Lee, H., Romero, J., Eds.; IPCC: Geneva, Switzerland, 2023; 184p. [CrossRef]
2. Mishra, A.K.; Singh, V.P. A review of drought concepts. *J. Hydrol.* **2010**, *391*, 202–216. [CrossRef]
3. Blauhut, V.; Stahl, K.; Stagge, J.H.; Tallaksen, L.M.; De Stefano, L.; Vogt, J. Estimating drought risk across Europe from reported drought impacts, drought indices, and vulnerability factors. *Hydrol. Earth Syst. Sci.* **2016**, *20*, 2779–2800. [CrossRef]
4. Kim, H.; Park, J.; Yoo, J.; Kim, T.-W. Assessment of drought hazard, vulnerability, and risk: A case study for administrative districts in South Korea. *J. Hydro-Environ. Res.* **2015**, *9*, 28–35. [CrossRef]
5. Hisdal, H.; Tallaksen, L.M. Estimation of regional meteorological and hydrological drought characteristics: A case study for Denmark. *J. Hydrol.* **2003**, *281*, 230–247. [CrossRef]
6. Teutschbein, C.; Jonsson, E.; Todorović, A.; Tootoonchi, F.; Stenfors, E.; Grabs, T. Future drought propagation through the water-energy-food-ecosystem nexus–A Nordic perspective. *J. Hydrol.* **2023**, *617*, 128963. [CrossRef]
7. Tuğrul, T.; Hinis, M.A. Trend analysis of hydrological and meteorological drought in Apa Dam, Türkiye. *Environ. Earth Sci.* **2024**, *83*, 502. [CrossRef]
8. Mustafa, A.M.; Barabadi, A. Criteria-Based Fuzzy Logic Risk Analysis of Wind Farms Operation in Cold Climate Regions. *Energies* **2022**, *15*, 1335. Available online: https://www.mdpi.com/1996-1073/15/4/1335 (accessed on 3 September 2024). [CrossRef]
9. Rousi, E.; Fink, A.H.; Andersen, L.S.; Becker, F.N.; Beobide-Arsuaga, G.; Breil, M.; Cozzi, G.; Heinke, J.; Jach, L.; Niermann, D.; et al. The extremely hot and dry 2018 summer in central and northern Europe from a multi-faceted weather and climate perspective. *Nat. Hazards Earth Syst. Sci.* **2023**, *23*, 1699–1718. [CrossRef]
10. Bakke, S.J.; Ionita, M.; Tallaksen, L.M. The 2018 northern European hydrological drought and its drivers in a historical perspective. *Hydrol. Earth Syst. Sci.* **2020**, *24*, 5621–5653. [CrossRef]
11. Suarez-Gutierrez, L.; Müller, W.A.; Marotzke, J. Extreme heat and drought typical of an end-of-century climate could occur over Europe soon and repeatedly. *Commun. Earth Environ.* **2023**, *4*, 415. [CrossRef]
12. Iversen, E.C.; Nygaard, B.E.; Hodnebrog, Ø.; Sand, M.; Ingvaldsen, K. Future projections of atmospheric icing in Norway. *Cold Reg. Sci. Technol.* **2023**, *210*, 103836. [CrossRef]
13. Laudon, H.; Spence, C.; Buttle, J.; Carey, S.K.; McDonnell, J.J.; McNamara, J.P.; Soulsby, C.; Tetzlaff, D. Save northern high-latitude catchments. *Nat. Geosci.* **2017**, *10*, 324–325. [CrossRef]
14. Pham, Q.B.; Abba, S.I.; Usman, A.G.; Linh, N.T.T.; Gupta, V.; Malik, A.; Costache, R.; Vo, N.D.; Tri, D.Q. Potential of Hybrid Data-Intelligence Algorithms for Multi-Station Modelling of Rainfall. *Water Resour. Manag.* **2019**, *33*, 5067–5087. [CrossRef]
15. Pérez-Alarcón, A.; Garcia-Cortes, D.; Fernández-Alvarez, J.C.; Martínez-González, Y. Improving Monthly Rainfall Forecast in a Watershed by Combining Neural Networks and Autoregressive Models. *Environ. Process.* **2022**, *9*, 53. [CrossRef]
16. Tuğrul, T.; Hinis, M.A. Improvement of drought forecasting by means of various machine learning algorithms and wavelet transformation. *Acta Geophys.* **2024**. [CrossRef]
17. Rezaei, M.; Moghaddam, M.A.; Azizyan, G.; Shamsipour, A.A. Prediction of agricultural drought index in a hot and dry climate using advanced hybrid machine learning. *Ain Shams Eng. J.* **2024**, *15*, 102686. [CrossRef]
18. Kumar, M.S.; Rajamani, D.; Nasr, E.A.; Balasubramanian, E.; Mohamed, H.; Astarita, A. A Hybrid Approach of ANFIS—Artificial Bee Colony Algorithm for Intelligent Modeling and Optimization of Plasma Arc Cutting on Monel™ 400 Alloy. *Materials* **2021**, *14*, 6373. Available online: https://www.mdpi.com/1996-1944/14/21/6373 (accessed on 3 September 2024). [CrossRef]
19. Oladipo, S.; Sun, Y. Enhanced adaptive neuro-fuzzy inference system using genetic algorithm: A case study in predicting electricity consumption. *SN Appl. Sci.* **2023**, *5*, 186. [CrossRef]
20. Rahmati, O.; Panahi, M.; Kalantari, Z.; Soltani, E.; Falah, F.; Dayal, K.S.; Mohammadi, F.; Deo, R.C.; Tiefenbacher, J.; Bui, D.T. Capability and robustness of novel hybridized models used for drought hazard modeling in southeast Queensland, Australia. *Sci. Total Environ.* **2020**, *718*, 134656. [CrossRef] [PubMed]
21. Pande, C.B.; Kushwaha, N.L.; Orimoloye, I.R.; Kumar, R.; Abdo, H.G.; Tolche, A.D.; Elbeltagi, A. Comparative Assessment of Improved SVM Method under Different Kernel Functions for Predicting Multi-scale Drought Index. *Water Resour. Manag.* **2023**, *37*, 1367–1399. [CrossRef]
22. Achite, M.; Katipoğlu, O.M.; Jehanzaib, M.; Elshaboury, N.; Kartal, V.; Ali, S. Hydrological Drought Prediction Based on Hybrid Extreme Learning Machine: Wadi Mina Basin Case Study, Algeria. *Atmosphere* **2023**, *14*, 1447. [CrossRef]
23. Achite, M.; Katipoglu, O.M.; Şenocak, S.; Elshaboury, N.; Bazrafshan, O.; Dalkılıç, H.Y. Modeling of meteorological, agricultural, and hydrological droughts in semi-arid environments with various machine learning and discrete wavelet transform. *Theor. Appl. Climatol.* **2023**, *154*, 413–451. [CrossRef]
24. Pande, C.B.; Sidek, L.M.; Varade, A.M.; Elkhrachy, I.; Radwan, N.; Tolche, A.D.; Elbeltagi, A. Forecasting of meteorological drought using ensemble and machine learning models. *Environ. Sci. Eur.* **2024**, *36*, 160. [CrossRef]
25. Latifoğlu, L.; Bayram, S.; Aktürk, G.; Citakoglu, H. Drought index time series forecasting via three-in-one machine learning concept for the Euphrates basin. *Earth Sci. Inform.* **2024**, *17*, 5841–5898. [CrossRef]
26. Talebi, H.; Samadianfard, S. Integration of machine learning and remote sensing for drought index prediction: A framework for water resource crisis management. *Earth Sci. Inform.* **2024**, *17*, 4949–4968. [CrossRef]

27. Dikshit, A.; Pradhan, B.; Alamri, A.M. Temporal Hydrological Drought Index Forecasting for New South Wales, Australia Using Machine Learning Approaches. *Atmosphere* **2020**, *11*, 585. Available online: https://www.mdpi.com/2073-4433/11/6/585 (accessed on 3 September 2024). [CrossRef]
28. Zhang, J.; Zhu, Y.; Zhang, X.; Ye, M.; Yang, J. Developing a Long Short-Term Memory (LSTM) based model for predicting water table depth in agricultural areas. *J. Hydrol.* **2018**, *561*, 918–929. [CrossRef]
29. Nandgude, N.; Singh, T.P.; Nandgude, S.; Tiwari, M. Drought Prediction: A Comprehensive Review of Different Drought Prediction Models and Adopted Technologies. *Sustainability* **2023**, *15*, 11684. Available online: https://www.mdpi.com/2071-1050/15/15/11684 (accessed on 2 September 2024). [CrossRef]
30. Márquez-Grajales, A.; Villegas-Vega, R.; Salas-Martínez, F.; Acosta-Mesa, H.-G.; Mezura-Montes, E. Characterizing drought prediction with deep learning: A literature review. *MethodsX* **2024**, *13*, 102800. [CrossRef]
31. Hochreiter, S.; Schmidhuber, J. Long Short-Term Memory. *Neural Comput.* **1997**, *9*, 1735–1780. [CrossRef]
32. Kratzert, F.; Klotz, D.; Brenner, C.; Schulz, K.; Herrnegger, M. Rainfall–runoff modelling using Long Short-Term Memory (LSTM) networks. *Hydrol. Earth Syst. Sci.* **2018**, *22*, 6005–6022. [CrossRef]
33. Villegas-Ch, W.; García-Ortiz, J.A. Long Short-Term Memory-Based Prototype Model for Drought Prediction. *Electronics* **2023**, *12*, 3956. Available online: https://www.mdpi.com/2079-9292/12/18/3956 (accessed on 1 September 2024). [CrossRef]
34. Wu, Z.; Yin, H.; He, H.; Li, Y. Dynamic-LSTM hybrid models to improve seasonal drought predictions over China. *J. Hydrol.* **2022**, *615*, 128706. [CrossRef]
35. Wang, T.; Tu, X.; Singh, V.P.; Chen, X.; Lin, K.; Zhou, Z. Drought prediction: Insights from the fusion of LSTM and multi-source factors. *Sci. Total Environ.* **2023**, *902*, 166361. [CrossRef]
36. Dikshit, A.; Pradhan, B.; Huete, A. An improved SPEI drought forecasting approach using the long short-term memory neural network. *J. Environ. Manag.* **2021**, *283*, 111979. [CrossRef] [PubMed]
37. Phetanan, K.; Hong, S.M.; Yun, D.; Lee, J.; Chotpantarat, S.; Jeong, H.; Cho, K.H. Enhancing flow rate prediction of the Chao Phraya River Basin using SWAT–LSTM model coupling. *J. Hydrol. Reg. Stud.* **2024**, *53*, 101820. [CrossRef]
38. Taylan, E.D. An Approach for Future Droughts in Northwest Türkiye: SPI and LSTM Methods. *Sustainability* **2024**, *16*, 6905. Available online: https://www.mdpi.com/2071-1050/16/16/6905 (accessed on 1 September 2024). [CrossRef]
39. Belayneh, A.; Adamowski, J.; Khalil, B.; Ozga-Zielinski, B. Long-term SPI drought forecasting in the Awash River Basin in Ethiopia using wavelet neural network and wavelet support vector regression models. *J. Hydrol.* **2014**, *508*, 418–429. [CrossRef]
40. Deo, R.C.; Şahin, M. Application of the Artificial Neural Network model for prediction of monthly Standardized Precipitation and Evapotranspiration Index using hydrometeorological parameters and climate indices in eastern Australia. *Atmos. Res.* **2015**, *161–162*, 65–81. [CrossRef]
41. Piri, J.; Abdolahipour, M.; Keshtegar, B. Advanced machine learning model for prediction of drought indices using hybrid SVR-RSM. *Water Resour. Manag.* **2023**, *37*, 683–712. [CrossRef]
42. Elbeltagi, A.; Pande, C.B.; Kumar, M.; Tolche, A.D.; Singh, S.K.; Kumar, A.; Vishwakarma, D.K. Prediction of meteorological drought and standardized precipitation index based on the random forest (RF), random tree (RT), and Gaussian process regression (GPR) models. *Environ. Sci. Pollut. Res.* **2023**, *30*, 43183–43202. [CrossRef] [PubMed]
43. Sihag, P.; Jain, P.; Kumar, M. Modelling of impact of water quality on recharging rate of storm water filter system using various kernel function based regression. *Model. Earth Syst. Environ.* **2018**, *4*, 61–68. [CrossRef]
44. Zarei, A.R.; Mahmoudi, M.R.; Moghimi, M.M. Determining the most appropriate drought index using the random forest algorithm with an emphasis on agricultural drought. *Nat. Hazards* **2023**, *115*, 923–946. [CrossRef]
45. En-Nagre, K.; Aqnouy, M.; Ouarka, A.; Naqvi, S.A.A.; Bouizrou, I.; El Messari, J.E.S.; Tariq, A.; Soufan, W.; Li, W.; El-Askary, H. Assessment and prediction of meteorological drought using machine learning algorithms and climate data. *Clim. Risk Manag.* **2024**, *45*, 100630. [CrossRef]
46. Partal, T.; Küçük, M. Long-term trend analysis using discrete wavelet components of annual precipitations measurements in Marmara region (Turkey). *Phys. Chem. Earth Parts A/B/C* **2006**, *31*, 1189–1200. [CrossRef]
47. Zhou, G.; Liu, X. Orthorectification Model for Extra-Length Linear Array Imagery. *IEEE Trans. Geosci. Remote Sens.* **2022**, *60*, 4709710. [CrossRef]
48. Beguería, S.; Vicente Serrano, S.M.; Reig-Gracia, F.; Latorre Garcés, B. *SPEIbase v.2.10 [Dataset]*; Version 2.10; DIGITAL.CSIC: Madrid, Spain, 2023. [CrossRef]
49. Afshar, M.H.; Bulut, B.; Duzenli, E.; Amjad, M.; Yilmaz, M. Global spatiotemporal consistency between meteorological and soil moisture drought indices. *Agric. For. Meteorol.* **2022**, *316*, 108848. [CrossRef]
50. Spinoni, J.; Antofie, T.; Barbosa, P.; Bihari, Z.; Lakatos, M.; Szalai, S.; Szentimrey, T.; Vogt, J. An overview of drought events in the Carpathian Region in 1961–2010. *Adv. Sci. Res.* **2013**, *10*, 21–32. [CrossRef]
51. Mehr, A.D.; Sorman, A.U.; Kahya, E.; Afshar, M.H. Climate change impacts on meteorological drought using SPI and SPEI: Case study of Ankara, Turkey. *Hydrol. Sci. J.* **2020**, *65*, 254–268. [CrossRef]
52. Wahla, S.S.; Kazmi, J.H.; Sharifi, A.; Shirazi, S.A.; Tariq, A.; Smith, H.J. Assessing spatio-temporal mapping and monitoring of climatic variability using SPEI and RF machine learning models. *Geocarto Int.* **2022**, *37*, 14963–14982. [CrossRef]
53. Wan, L.; Bento, V.A.; Qu, Y.; Qiu, J.; Song, H.; Zhang, R.; Wu, X.; Xu, F.; Lu, J.; Wang, Q. Drought characteristics and dominant factors across China: Insights from high-resolution daily SPEI dataset between 1979 and 2018. *Sci. Total Environ.* **2023**, *901*, 166362. [CrossRef] [PubMed]

54. Ahmadalipour, A.; Moradkhani, H.; Demirel, M.C. A comparative assessment of projected meteorological and hydrological droughts: Elucidating the role of temperature. *J. Hydrol.* **2017**, *553*, 785–797. [CrossRef]
55. Hao, Z.; Singh, V.P. Drought characterization from a multivariate perspective: A review. *J. Hydrol.* **2015**, *527*, 668–678. [CrossRef]
56. Haro-Monteagudo, D.; Daccache, A.; Knox, J. Exploring the utility of drought indicators to assess climate risks to agricultural productivity in a humid climate. *Hydrol. Res.* **2018**, *49*, 539–551. [CrossRef]
57. Vicente-Serrano, S.M.; Beguería, S.; López-Moreno, J.I.; Angulo, M.; El Kenawy, A. A new global 0.5 gridded dataset (1901–2006) of a multiscalar drought index: Comparison with current drought index datasets based on the Palmer Drought Severity Index. *J. Hydrometeorol.* **2010**, *11*, 1033–1043. [CrossRef]
58. Beguería, S.; Serrano, S.M.V.; Reig-Gracia, F.; Garcés, B.L. Standardized precipitation evapotranspiration index (SPEI) revisited: Parameter fitting, evapotranspiration models, tools, datasets and drought monitoring. *Int. J. Climatol.* **2014**, *34*, 3001–3023. [CrossRef]
59. Allen, R.G.; Pereira, L.S.; Raes, D.; Smith, M. *Crop Evapotranspiration—Guidelines for Computing Crop Water Requirements—FAO Irrigation and Drainage Paper 56*; FAO: Rome, Italy, 1998; Volume 300, p. D05109.
60. Trajkovic, S.; Gocic, M.; Pongracz, R.; Bartholy, J. Adjustment of Thornthwaite equation for estimating evapotranspiration in Vojvodina. *Theor. Appl. Climatol.* **2019**, *138*, 1231–1240. [CrossRef]
61. Mikolov, T.; Joulin, A.; Chopra, S.; Mathieu, M.; Ranzato, M.A. Learning longer memory in recurrent neural networks. *arXiv* **2014**, arXiv:1412.7753.
62. Boser, B.E.; Guyon, I.M.; Vapnik, V.N. A training algorithm for optimal margin classifiers. In Proceedings of the Fifth Annual Workshop on Computational Learning Theory, New York, NY, USA, 27–29 July 1992; pp. 144–152.
63. Oruc, S.; Tugrul, T.; Hinis, M.A. Beyond Traditional Metrics: Exploring the Potential of Hybrid Algorithms for Drought Characterization and Prediction in the Tromso Region, Norway. *Appl. Sci.* **2024**, *14*, 7813. [CrossRef]
64. Shabani, E.; Ghorbani, M.A.; Inyurt, S. The power of the GP-ARX model in CO_2 emission forecasting. In *Risk, Reliability and Sustainable Remediation in the Field of Civil and Environmental Engineering*; Elsevier: Amsterdam, The Netherlands, 2022; pp. 79–91.
65. Katipoğlu, O.M.; Yeşilyurt, S.N.; Dalkılıç, H.Y.; Akar, F. Application of empirical mode decomposition, particle swarm optimization, and support vector machine methods to predict stream flows. *Environ. Monit. Assess.* **2023**, *195*, 1108. [CrossRef]
66. Saha, S.; Saha, A.; Hembram, T.K.; Kundu, B.; Sarkar, R. Novel ensemble of deep learning neural network and support vector machine for landslide susceptibility mapping in Tehri region, Garhwal Himalaya. *Geocarto Int.* **2022**, *37*, 17018–17043. [CrossRef]
67. Muller, K.-R.; Mika, S.; Ratsch, G.; Tsuda, K.; Scholkopf, B. An Introduction to Kernel-Based Learning Algorithms. *IEEE Trans. Neural Netw.* **2001**, *12*, 181–201. [CrossRef] [PubMed]
68. Abumohsen, M.; Owda, A.Y.; Owda, M.; Abumihsan, A. Hybrid machine learning model combining of CNN-LSTM-RF for time series forecasting of Solar Power Generation. *e-Prime-Adv. Electr. Eng. Electron. Energy* **2024**, *9*, 100636. [CrossRef]
69. Gunn, S.R. *Support Vector Machines for Classification and Regression*; Citeseer: Princeton, NJ, USA, 1997.
70. Vapnik, V.N. An overview of statistical learning theory. *IEEE Trans. Neural Netw.* **1999**, *10*, 988–999. [CrossRef] [PubMed]
71. Panahi, M.; Sadhasivam, N.; Pourghasemi, H.R.; Rezaie, F.; Lee, S. Spatial prediction of groundwater potential mapping based on convolutional neural network (CNN) and support vector regression (SVR). *J. Hydrol.* **2020**, *588*, 125033. [CrossRef]
72. Belayneh, A.; Adamowski, J.; Khalil, B. Short-term SPI drought forecasting in the Awash River Basin in Ethiopia using wavelet transforms and machine learning methods. *Sustain. Water Resour. Manag.* **2016**, *2*, 87–101. [CrossRef]
73. Ghasemi, P.; Karbasi, M.; Nouri, A.Z.; Tabrizi, M.S.; Azamathulla, H.M. Application of Gaussian process regression to forecast multi-step ahead SPEI drought index. *Alex. Eng. J.* **2021**, *60*, 5375–5392. [CrossRef]
74. Neal, R.M. Monte Carlo implementation of Gaussian process models for Bayesian regression and classification. *arXiv* **1997**, arXiv:physics/9701026.
75. Likar, B.; Kocijan, J. Predictive control of a gas–liquid separation plant based on a Gaussian process model. *Comput. Chem. Eng.* **2007**, *31*, 142–152. [CrossRef]
76. Jamei, M.; Ahmadianfar, I.; Olumegbon, I.A.; Karbasi, M.; Asadi, A. On the assessment of specific heat capacity of nanofluids for solar energy applications: Application of Gaussian process regression (GPR) approach. *J. Energy Storage* **2021**, *33*, 102067. [CrossRef]
77. Khan, M.H.A.; Jafri, T.H.; Ud-Din, S.; Ullah, H.S.; Nawaz, M.N. Prediction of soil compaction parameters through the development and experimental validation of Gaussian process regression models. *Environ. Earth Sci.* **2024**, *83*, 129. [CrossRef]
78. Elbeltagi, A.; Azad, N.; Arshad, A.; Mohammed, S.; Mokhtar, A.; Pande, C.; Etedali, H.R.; Bhat, S.A.; Islam, A.R.M.T.; Deng, J. Applications of Gaussian process regression for predicting blue water footprint: Case study in Ad Daqahliyah, Egypt. *Agric. Water Manag.* **2021**, *255*, 107052. [CrossRef]
79. Breiman, L. Random Forests. *Mach. Learn.* **2001**, *45*, 5–32. [CrossRef]
80. Shang, K.; Xu, L.; Liu, X.; Yin, Z.; Liu, Z.; Li, X.; Yin, L.; Zheng, W. Study of urban heat island effect in Hangzhou metropolitan area based on SW-TES algorithm and image dichotomous model. *Sage Open* **2023**, *13*, 21582440231208851. [CrossRef]
81. Choi, C.; Kim, J.; Han, H.; Han, D.; Kim, H.S. Development of water level prediction models using machine learning in wetlands: A case study of Upo wetland in South Korea. *Water* **2019**, *12*, 93. [CrossRef]
82. Jiao, K.; Han, D.; Li, J.; Bai, B.; Gong, L.; Yu, B. A novel LBM-DEM based pore-scale thermal-hydro-mechanical model for the fracture propagation process. *Comput. Geotech.* **2021**, *139*, 104418. [CrossRef]
83. Biau, G.; Scornet, E. A random forest guided tour. *Test* **2016**, *25*, 197–227. [CrossRef]

84. Yu, P.-S.; Yang, T.-C.; Chen, S.-Y.; Kuo, C.-M.; Tseng, H.-W. Comparison of random forests and support vector machine for real-time radar-derived rainfall forecasting. *J. Hydrol.* **2017**, *552*, 92–104. [CrossRef]
85. Tyralis, H.G. Papacharalampous, and A. Langousis, A brief review of random forests for water scientists and practitioners and their recent history in water resources. *Water* **2019**, *11*, 910. [CrossRef]
86. Kisi, O. Wavelet regression model as an alternative to neural networks for river stage forecasting. *Water Resour. Manag.* **2011**, *25*, 579–600. [CrossRef]
87. Kisi, O.; Cimen, M. A wavelet-support vector machine conjunction model for monthly streamflow forecasting. *J. Hydrol.* **2011**, *399*, 132–140. [CrossRef]
88. Maheswaran, R.; Khosa, R. Comparative study of different wavelets for hydrologic forecasting. *Comput. Geosci.* **2012**, *46*, 284–295. [CrossRef]
89. Sang, Y.-F. A review on the applications of wavelet transform in hydrology time series analysis. *Atmos. Res.* **2013**, *122*, 8–15. [CrossRef]
90. Mallat, S.G. A theory for multiresolution signal decomposition: The wavelet representation. *IEEE Trans. Pattern Anal. Mach. Intell.* **1989**, *11*, 674–693. [CrossRef]
91. Khan, M.M.H.; Muhammad, N.S.; El-Shafie, A. Wavelet based hybrid ANN-ARIMA models for meteorological drought forecasting. *J. Hydrol.* **2020**, *590*, 125380. [CrossRef]
92. Zhang, D. A Coefficient of Determination for Generalized Linear Models. *Am. Stat.* **2017**, *71*, 310–316. [CrossRef]
93. Yilmaz, V.; Koycegiz, C.; Buyukyildiz, M. An approach on the estimation and temporal interaction of runoff: The band similarity method. *J. Water Clim. Chang.* **2024**, *15*, 4775–4789. [CrossRef]
94. Ehteram, M.; Ahmed, A.N.; Ling, L.; Fai, C.M.; Latif, S.D.; Afan, H.A.; Banadkooki, F.B.; El-Shafie, A. Pipeline scour rates prediction-based model utilizing a multilayer perceptron-colliding body algorithm. *Water* **2020**, *12*, 902. [CrossRef]
95. Mohammed, S.; Elbeltagi, A.; Bashir, B.; Alsafadi, K.; Alsilibe, F.; Alsalman, A.; Zeraatpisheh, M.; Széles, A.; Harsányi, E. A comparative analysis of data mining techniques for agricultural and hydrological drought prediction in the eastern Mediterranean. *Comput. Electron. Agric.* **2022**, *197*, 106925. [CrossRef]
96. Aktürk, G.; Çıtakoğlu, H.; Demir, V.; Beden, N. Meteorological Drought Analysis and Regional Frequency Analysis in the Kızılırmak Basin: Creating a Framework for Sustainable Water Resources Management. *Water* **2024**, *16*, 2124. Available online: https://www.mdpi.com/2073-4441/16/15/2124 (accessed on 30 August 2024). [CrossRef]
97. Hinis, M.A.; Geyikli, M.S. Accuracy Evaluation of Standardized Precipitation Index (SPI) Estimation under Conventional Assumption in Yeşilırmak, Kızılırmak, and Konya Closed Basins, Turkey. *Adv. Meteorol.* **2023**, *2023*, 5142965. [CrossRef]
98. Coşkun, Ö.; Citakoglu, H. Prediction of the standardized precipitation index based on the long short-term memory and empirical mode decomposition-extreme learning machine models: The Case of Sakarya, Türkiye. *Phys. Chem. Earth Parts A/B/C* **2023**, *131*, 103418. [CrossRef]
99. Achite, M.; Simsek, O.; Sankaran, A.; Katipoğlu, O.M.; Caloiero, T. Analyzing the dynamical relationships between meteorological and hydrological drought of Wadi Mina basin, Algeria using a novel multiscale framework. *Stoch. Environ. Res. Risk Assess.* **2024**, *38*, 1935–1953. [CrossRef]
100. Citakoglu, H.; Coşkun, Ö. Comparison of hybrid machine learning methods for the prediction of short-term meteorological droughts of Sakarya Meteorological Station in Turkey. *Environ. Sci. Pollut. Res.* **2022**, *29*, 75487–75511. [CrossRef] [PubMed]
101. Karbasi, M.; Karbasi, M.; Jamei, M.; Malik, A.; Azamathulla, H.M. Development of a new wavelet-based hybrid model to forecast multi-scalar SPEI drought index (case study: Zanjan city, Iran). *Theor. Appl. Climatol.* **2022**, *147*, 499–522. [CrossRef]
102. Poornima, S.; Pushpalatha, M. Drought prediction based on SPI and SPEI with varying timescales using LSTM recurrent neural network. *Soft Comput.* **2019**, *23*, 8399–8412. [CrossRef]